Formation of Saturn and Distribution of its Growth Times

A thesis

submitted to

Indian Institute of Science Education and Research, Pune

Earth and Climate Sciences Department

in partial fulfillment of the requirements for the

BS-MS Dual Degree Programme

by

Anuja Deepak Raorane

Indian Institute of Science Education and Research Pune

Dr. Homi Bhabha Road,

Pashan, Pune 411008, INDIA.

April 2023

Supervisor: Dr. Ramon Brasser

CERTIFICATE

This is to certify that this dissertation entitled **"Formation of Saturn and Distribution of its Growth Times"** towards the partial fulfillment of the BS-MS dual degree program at the Indian Institute of Science Education and Research, Pune, represents study/work carried out by **Anuja Deepak Raorane** at Indian Institute of Science Education and Research Pune, and and Konkoly Observatory of the Research Center of Astronomy and Earth Sciences Budapest, under the supervision of **Dr. Ramon Brasser**, Research Fellow, Konkoly Observatory of the Research Center for Astronomy and Earth Sciences, during the academic year **2022-23**.

Anuja Raorane **Ramon Brasser**

Committee:

Supervisor: Dr. Ramon Brasser

TAC Member: Dr. Shreyas Managave

Place: Pune Date: 25/04/23

DECLARATION

I, **Anuja Deepak Raorane**, hereby declare that the research work presented in the report entitled **"Formation of Saturn and Distribution of its Growth Times"** has been carried out by me at the **Department of Earth and Climate Sciences**, Indian Institute of Science Education and Research Pune, and Konkoly Observatory of the Research Center of Astronomy and Earth Sciences Budapest, under the supervision of **Dr. Ramon Brasser**, and the same has not been submitted elsewhere for any other degree.

Anuja Raorane | **Ramon Brasser**

Place: Pune | Date: 25/04/23

This thesis is dedicated to my Aajji who always encouraged me to pursue my dreams.

ACKNOWLEDGEMENTS

I would like to express my heartfelt gratitude to everyone who has been instrumental in making my master's thesis work a success. First and foremost, I extend my sincere thanks to my supervisor, Dr. Ramon Brasser, for his constant support, guidance, and overall mentoring throughout the project. His valuable insights and constructive feedback have been invaluable in shaping my research work. I would also like to acknowledge my expert, Dr. Shreyas Managave, for his support.

I sincerely thank Mr. Swapnil Bhuktar for his cooperative response and for making my travel to Budapest possible. I would also like to acknowledge the director Dr.Robert Szabo, the HR department, IT department and others at the Konkoly Observatory, Budapest for making my stay there smooth and comfortable. I offer my sincerest thanks to Lucy and Emily for extending to me their warmest hospitality and making me feel right at home amidst their midst.

I would like to express my heartfelt thanks to Dr. Sudha Rajamani, who has been a constant support throughout my IISER journey. Her encouragement and guidance have been a source of inspiration for me. I am also grateful to the ECS department at IISER Pune for giving me the opportunity to work on this project. I extend my gratitude to Saurabh Butolia and the members of the IT department for granting me the access to VPN, thereby enabling me to connect with Parambrahma. I acknowledge the Kishore Vaigyanik Protsahan Yojana (KVPY) for the scholarship.

I would like to express my gratitude to Dr. Lee Man Hoi for his invaluable contribution in initiating the idea of giant planet formation. Additionally, I extend my heartfelt thanks to Dr. Soko Matsumura for her remarkable work in creating the pebble accretion SyMBA, which is the soul of my thesis. Last but not least, I would like to acknowledge Tommy for his efforts in optimizing SyMBA and making it significantly faster, thus enabling more efficient and accurate simulations.

Purva, Goirik, and Chincholi, thank you for your unwavering support and encouragement throughout my academic journey at IISER. I really appreciate your patience and support in addressing all my silly computer queries. Your words of encouragement, ”ho jaayega Anuja,” gave me the confidence to embark on a computational project that I wouldn’t have dared to take otherwise. I am grateful to my brother, Shreyas, for his assistance whenever my computer malfunctioned, despite his reputation as a troublemaker. My sincerest thanks to Rabin for his unwavering support through thick and thin. His guidance and encouragement have been a source of inspiration to me.

Lastly, I would like to thank my parents, relatives and all my friends, without their encouragement, this journey would have been impossible. Their support has been a constant source of motivation, and I am deeply grateful for their unwavering belief in me.

ABSTRACT

The work presented here encompasses the intriguing evolution of our celestial neighborhood, the solar system. This study centers on the formation of giant planets in the outer region of the solar system. Apart from the Cassini mission to Saturn, Jupiter has garnered the majority share of research attention, leaving little room for inquiry into the formation and evolution of its lesser-explored counterpart, Saturn. This project aims to investigate the conditions and parameters of the protoplanetary disk that led to the formation of Saturn and its distribution of formation times. The study explores the implications of the simplest disc and pebble accretion model, with steady-state accretion, on the formation of gas giants.

We conducted a statistical survey of different disk parameters and initial conditions to establish which combination best reproduces the present outer solar system. The parameter space is large: we examined the effect of the initial planetesimal disk mass, the number of planetesimals and their size-frequency distribution, the coagulation, and dust-settling timescales, planet migration, and the feedback of gas disk that will govern the overall dynamics of the final sizes, compositions, and positions of the planets. The results reveal that pebble accretion is sensitive to various parameters and initial conditions of the disk, and in the absence of a planetesimal disk, the giant planets will be highly eccentric. Moreover, it is challenging to replicate the formation of all four giant planets in the outer solar system in a single simulation. The study estimates the average formation time for Saturn to be $\langle t_{\mathrm{Saturn}} \rangle = 3.09 \pm 1.33$ Myrs, which aligns closely with the Hf-W reset age of the Eagle Station pallasite, an achondritic meteorite from the outer solar system.

This study plays a pivotal role in understanding the configuration of the contemporary solar system as we perceive it. The emergence of gas giants in the outer solar system bears implications for the inflow of matter towards the inner regions, influencing the terrestrial planets and the makeup of the asteroid and Kuiper belts. This work contributes to the dynamic evolution of these planets, which are responsible for molding the composition of the inner solar system and the terrestrial planets.

Contents

List of Figures

List of Tables

Introduction

Our Solar System, as we know it today, is 4.568 billion years old. The Solar System, including its planetary bodies, moons, and asteroid belt, was formed within 100 million years after the formation of the sun[1]. The protoplanetary disk surrounding the young Sun formed as a consequence of angular momentum conservation during the star formation process. The flattened rotating disk was heated by viscous evolution, and the protostar and its evolution consequently provided the material (gas, dust, and solid material) and location to form the planets. Accretion processes, migration, and gas drag resulted in forming of planets and other solar system objects[2]. The Solar System's gas giants, Jupiter and Saturn, could have been the first-formed planets because the timescale of gas dissipation constrains their formation. Jupiter, the most giant planet with a mass of about 315 Earth masses, is at a distance of 5 AU from the sun. Saturn, the second largest planet, with 95 Earth masses, is 9.5 AU from the Sun.

1.1 Existing Models on Gas giant formation

There have been several propositions on how these gas giants formed. In the gas collapse model[3], a gravitationally unstable disk fragments directly into self-gravitating clumps of gas and dust that can contract and become giant gaseous protoplanets. The core accretion model[4] suggests that the formation of Jupiter and Saturn began with the accumulation of solid particles, such as dust and ice, in the protoplanetary disk, leading to the formation of planetesimals. As the planetesimals grew in size, their gravitational attraction became strong enough to attract other particles, leading to even more growth to become planetary embryos. As this core grows, it acquires a growing atmosphere of nebular gas, which eventually becomes unstable to collapse, leading to a phase of rapid accretion of hydrogen and helium gas onto the protoplanet's envelope[3].

As per the current theory of planetary accretion, it is estimated that a 5 Earth-mass core would take around 50 Myr and 300 Myr to form at Jupiter's and Saturn's regions[5], respectively. These timescales are longer than the inferred lifetime of nebular gas, which is between 0.1 Myr and 10 Myr, as determined from observations of young stars similar to the Sun[6]. Moreover, Levison et al. (2010)[7] have shown that in the outer solar system, this leads to the early migration of the cores of the gas giants (planetesimal-driven migration), forming many hot super-earths and gas giants. In a later study, Levison et al. (2015)[8] analyzed whether pebble accretion could be responsible for the formation of the gas giants, and they concluded that this appeared to be a viable mechanism. The idea is similar to the core accretion model, but pebbles (a few km-sized objects) are accreted instead of planetesimals, resulting in a faster core formation. According to Matsumura et al. (2021)[9], pebble accretion could be responsible for the immense diversity of exoplanetary systems since it's more sensitive to different disk conditions than planetesimal accretion.

1.2 Purpose and Implication of this Study

Over the years, the formation of Jupiter has been of interest due to its ability to shape the Solar System's history. Still, not much attention has been given to the formation and growth of Saturn and its migration. Saturn has 95 Earth masses ($M_\oplus$), while Jupiter has over 300 $M_\oplus$. This incites us to ask why Saturn stopped accreting gas at 95 AU while Jupiter continued to grow if the same physics governed the process of gas accretion and annulus formation.

In this work, the implications of the simplest disc and pebble accretion model are being investigated, with steady-state accretion onto the star and no ringed structures in the disc because the effect of a ringed structure in the disc on pebble accretion is not yet well understood. It is further assumed that no additional material is added to the disc from the interstellar medium as it evolves. A statistical survey of different disk parameters and initial conditions is performed to see which best reproduces the present solar system. The simulation data is further validated by showing Saturn's formation time and if it compares well to reset ages of carbonaceous achondrite meteorites such as Eagle Station.

Meteorite isotopic anomalies and ages suggest that Jupiter's core was constructed mainly from first-generation planetesimals, like the parent body of the Eagle Station pallasites, iron meteorites, and carbonaceous chondrites. Recent studies involving Hf-W age dating[10] and Mo isotopic[11] composition demonstrate that the Eagle Station originates from the outer disk (carbonaceous chondrite reservoir). According to Raymond and Izidoro (2017)[12], there was a constant shuffling of scattered material between Jupiter and Saturn. We expect that this process generated a high impact on the particles between them, and the Hf-W core formation age of (2.7 ± 1.2) Myr after CAI for the Eagle Station pallasite is a result of that. We believe this metallic meteorite constrains Saturn's formation time, but this is only a working hypothesis that requires further testing in future work.

Gas giant formation leads to a cascade of events in our solar system. Since they are likely the first planets to form, they influence the rest of the dynamics. The inward migration of pebbles and other particles from the outer to the inner solar system may be regulated by several factors, including the gravitational influence of giant planets. Such regulation may significantly affect the composition of the inner solar system[10]. Additionally, the scattering of planetesimals may impact the density of the asteroid belt and Kuiper belt, as well as migration, thus influencing the process of late accretion. The combined effects of these phenomena may have played a critical role in the formation and evolution of the solar system as we observe it today.

Theory

2.1 Gas Disk

Accretion is a radial flow of gas onto a central object driven by angular momentum transfer. In a deferentially rotating medium, tangential stresses between adjacent layers, which are connected with the existence of the magnetic field, turbulence, and radiative and molecular viscosity, are the mechanisms of transfer of angular momentum[13]. The disc evolution is described by the diffusion equation[9] for the disc's surface mass density Σ_g:

$$\frac{\partial \Sigma_g}{\partial t} = -\frac{1}{r}\frac{\partial}{\partial r}\left[3r^{1/2}\frac{\partial}{\partial r}(\Sigma_g \nu r^{1/2})\right] \tag{2.1}$$

where ν is the disc's 'viscosity' representing the accretion. The viscosity can be transformed to a parameter α that denotes the accretion strength due to the disturbances in the disk.

The circumstellar disk that encircled the nascent Sun promptly materialized following its formation, comprised predominantly of a gaseous component. This circumstellar disk, commonly referred to as a protostellar disk, was primarily constituted by gas and dust and played a fundamental role in the subsequent evolution of the Sun and the formation of the planetary system.

2.1.1 Gas Accretion

Gas accretion is the process by which gas particles are gravitationally drawn into the gravitational well of a forming planet, eventually coalescing into a larger and larger body. The gas accretion rate onto the star[14], $\dot{M}_*$ is related to the gas surface density, Σ, and scale height of the disc, H, via

$$\dot{M}_* = 3\pi\alpha_{\rm acc}\Sigma H^2\Omega_{\rm K}, \tag{2.2}$$

where $\Omega_{\rm K} = \sqrt{GM_\odot/r^3}$ is the Kepler frequency. The parameter $\alpha_{\rm acc}$ is a measure for the global angular momentum transfer of the disc, which is assumed to be constant and comes from the disc viscosity[15] $\nu = \alpha_{\rm acc}c_s^2\Omega_{\rm K}$. The disc scale height $H = c_s/\Omega_{\rm K}$, where $c_{\rm s}^2 = (\gamma k_B T/2.3m_p)$ is the sound speed, $k_B = 1.381 \times 10^{-23}$ m^2 kg s^{-1} K^{-2} is the Boltzmann constant, m_p is the proton mass, the mean atomic mass of the gas is assumed to be 2.3 and γ is the ratio of specific heats of the gas molecules. The stellar accretion rate[16] decreases with time as

$$\dot{M}_* = \frac{M_d}{(2q+1)t_{\rm diff}}\left(\frac{t}{t_{\rm diff}}+1\right)^{-(2q_2+2)/(2q_2+1)} \tag{2.3}$$

where M_d is the mass of the disc, $t_{\rm diff}$ is the diffusion time, and $q_2 = -{\rm d}\ln T/{\rm d}\ln r$ is the negative temperature gradient in the irradiative regime of the disc in the giant planet region. In most of the disc $q_2 = 3/7$ (refer 2.4) and $-(2q_2+2)/(2q_2+1) = -20/13 \approx -1.53$. Most observed discs have a mass that's about 3%-8% of the stellar mass[17]. For a disc mass of $M_d = 0.05\ M_\odot$ we have initially $\dot{M}_{*8} = 5.3$ if $t_{\rm diff} = 0.5$ Myr.

In the giant planet region, the disc the mid-plane temperature can be approximated by[18]

$$T = 150\left(\frac{L_*}{L_\odot}\right)^{2/7}\left(\frac{M_*}{M_\odot}\right)^{-1/7}\left(\frac{r}{1\,{\rm au}}\right)^{-3/7}\ {\rm K}, \tag{2.4}$$

where r is the distance to the Sun. To simplify the formulae, we define

$$\alpha_3 \equiv \frac{\alpha_{\rm acc}}{10^{-3}}, \tag{2.5}$$

$$\dot{M}_{*8} \equiv \frac{\dot{M}_*}{10^{-8}\, M_\odot\, {\rm yr}^{-1}}. \tag{2.6}$$

With this temperature profile, one may compute the reduced scale height $h = H/r$ as

$$h = 0.029\Big(\frac{L_*}{L_\odot}\Big)^{1/7}\Big(\frac{M_*}{M_\odot}\Big)^{-4/7}\Big(\frac{r}{1\,{\rm au}}\Big)^{2/7}. \tag{2.7}$$

The gas surface density is

$$\Sigma = 1785\Big(\frac{L_*}{L_\odot}\Big)^{-2/7}\Big(\frac{M_*}{M_\odot}\Big)^{9/14}\alpha_3^{-1}\dot{M}_{*8}\Big(\frac{r}{1\,{\rm au}}\Big)^{-15/14}\,{\rm g\,cm^{-2}}. \tag{2.8}$$

The so-called snow line is defined by the distance to the star where the mid-plane temperature $T \sim 170$ K, which is at

$$r_{\rm s} = 0.75\Big(\frac{L_*}{L_\odot}\Big)^{2/3}\Big(\frac{M_*}{M_\odot}\Big)^{-1/3}\,{\rm au}. \tag{2.9}$$

The nucleated instability model[19] proposes that the formation of giant planets may occur when a solid protoplanet, commonly referred to as a core, reaches a critical mass and triggers rapid accretion of nebular gas, resulting in the formation of a massive gaseous envelope. The growth time of the gaseous envelope mass τ_g depends strongly on the core mass of the planet, moderately on the grain opacity, and weakly on the past core accretion process[19].

$$\tau_g = b\Big(\frac{M_{\rm core}}{M_\oplus}\Big)^{-c}\Big(\frac{\kappa_{\rm gr}}{1\,{\rm cm^2\,g^{-1}}}\Big)\,{\rm yr} \tag{2.10}$$

where $M_{\rm core}$ is the core mass and κ_{gr} is the grain opacity.

2.1.2 Gas Dissipation

Gas dissipation during early solar system formation is a critical process that influences the evolution of planetary systems. It refers to the gradual loss of gas from the protoplanetary disk that surrounds a young star, which is thought to occur on a timescale of a few million years. As the gas dissipates, the disk becomes less massive and less dense, which in turn affects the way that gas accretes onto the forming planets[9].

$$t_{\rm diff} \equiv \frac{1}{3(q_2+1/2)^2}\frac{r_D^2}{\nu_D} \tag{2.11}$$

where r_D is the characteristic disc size, ν_D is the corresponding viscosity.

2.2 Pebble Accretion

Pebble accretion is a process that is thought to occur when the young star is still surrounded by its protoplanetary disk consisting of gas and solids. Here I briefly outline the assumed disc model.

2.2.1 Pebble accretion onto planetesimals

Ida et al. (2018)[20] and Matsumura et al. (2020)[21] have proposed a model that accounts for planet-disk interactions, type II migration, and the two-α model. The incorporation of these factors has led to efficient accretion, thereby enabling the formation of gas giant cores through pebble accretion within a time frame of 5 million years. The rate of accretion from pebbles onto a planetesimal-sized or larger body is derived to be[18]

$$\dot{M}_{\rm core} = \varepsilon \dot{M}_F, \tag{2.12}$$

where $\dot{M}_F$ is the pebble mass flux. The accretion efficiency ε is given by[18]

$$\varepsilon = \min\Big[1, \frac{C\hat{b}^2\sqrt{1+4\mathcal{S}^2}}{4\sqrt{2\pi}\mathcal{S}\hat{h}_p}\Big(1+\frac{3\hat{b}}{2\chi\eta}\Big)\Big], \tag{2.13}$$

where $\dot{M}_F$ is the flux of pebbles through the disk; its temporal evolution depends on the gas accretion rate onto the star and the formation efficiency of pebbles. The other quantities in equation (2.13) are given by

$$
\begin{aligned}
b &= 2\kappa r_H \mathcal{S}^{1/3} \min\Big(\sqrt{\frac{3r_H}{\chi\eta r}}\mathcal{S}^{1/6}, 1\Big), \\
\chi &= \frac{\sqrt{1+4\mathcal{S}^2}}{1+\mathcal{S}^2}, \\
h_p &= \Big(1+\frac{\mathcal{S}}{\alpha_t}\Big)^{-1/2} h \\
C &= \min\Big(\sqrt{\frac{8}{\pi}}\frac{h_p}{b}, 1\Big), \\
\eta &= \frac{1}{2}h^2\Big|\frac{d\ln P}{d\ln r}\Big| \approx 1.3h^2 \\
\ln\kappa &= -\bigg(\frac{\mathcal{S}}{\mathcal{S}^*}\bigg)^{0.65}, \\
\mathcal{S}^* &= \min\big[2, 4\eta^{-3}\mu\big]
\end{aligned}
$$

where G is the gravitational constant, $\mu = m/M_*$, where m is the mass of the planet/planetesimal, M_* is the mass of the star, α_t is the disk's turbulent viscosity, $r_H = r(\mu/3)^{1/3}$ is the Hill radius, P is the gas pressure and $\mathcal{S}$ is the Stokes number. Quantities with a circumflex are scaled by the distance to the star, and h_p is the scale height of the pebbles as they drift sunward through the disc.

An alternative for the pebble accretion efficiency is given by Ormel and Liu (2018)[22], who included combined effects of the planet's gravitational attraction and gas drag in their prescription. They studied the 3D pebble accretion efficiency by considering the effects of eccentricity, inclination, and disc turbulence. When the planetesimal is small compared to the scale height of the pebble stream, the accretion efficiency is given by

$$
\varepsilon = \frac{A_3}{\eta h_{\mathrm{p,eff}}}\Big(\frac{m_p}{M_*}\Big) f_{\mathrm{set}}^2 \tag{2.14}
$$

where $A_3 = 0.39$ is a constant, $h_{\mathrm{p,eff}}$ is the effective pebble scale height, and $f_{\mathrm{set}} = \exp[-0.5(\Delta v/v_*)^2]$ is the settling fraction, with Δv the approach speed between the pebble and the planetesimal, and $v_* = (m_p/M_*)^{1/3}\mathcal{S}^{-1/3}v_K$, where $v_K = r\Omega_K$ is the Kepler velocity. When the planetesimal mass grows large enough such that its diameter becomes comparable to the pebble scale height, the efficiency becomes

$$\varepsilon = \frac{A_2}{\eta}\left[\frac{m_p}{M_*}\frac{\Delta v}{v_*}\mathcal{S}^{-1}\right]^{1/2} f_{\rm set}, \tag{2.15}$$

where $A_2 = 0.32$. These are complicated functions of the planetesimal inclination and eccentricity, and we refer to Ormel & Liu (2018) for more details.

Pebble accretion causes rapid growth onto planetesimals with diameters of some 200 km or greater[23]. The pebble mass flux describes the pebble mass swept up by the pebble formation front per unit time through the disk[9],

$$\dot{M}_F = 2\pi r_{\rm pff}\Sigma_p \frac{dr_{\rm pff}}{dt} \tag{2.16}$$

where Σ_p is the pebble surface density in the pebble migrating region.

The pebbles are formed in a front that sweeps outwards as the gas disc cools[24]. The timescale of growth from μm-sized grains to pebbles (by several orders of magnitude in radius), $t_{\rm grow,peb}$ has a sensitive r-dependence. This results in an "inside out formation" of pebbles; formation is earlier in the inner region, and the formation front migrates outward[18]. The pebble formation time, $t_{\rm pff}$, is the time at which the pebble formation front reaches the characteristic disk radius, $r_{d,0}$, and $r_{\rm pff}$ is the radius of the pebble formation front. These two quantities are computed as[18].

$$r_{\rm pff} = 100 f^{2/3}\left(\frac{t}{2\times 10^5\,{\rm yr}}\right)^{2/3}\left(\frac{Z_0}{10^{-2}}\right)^{2/3}\left(\frac{M_*}{M_\odot}\right)^{1/3}{\rm au} \tag{2.17}$$

$$t_{\rm pff} = 2 f^{-1}\times 10^5\left(\frac{Z_0}{10^{-2}}\right)^{-1}\left(\frac{r_{d,0}}{100\,{\rm au}}\right)^{3/2}\left(\frac{M_*}{M_\odot}\right)^{-1/2}{\rm yr} \tag{2.18}$$

where Z_0 is the initial solid-to-gas ratio in the disk and is typically assumed to be 0.01, f is the sticking efficiency of dust to pebbles, and is an input parameter.

Now one can compute the flux of pebbles in the disc. I used the derivation by Matsumura et al. (2021)[9], which yields.

$$\dot{M}_F = 0.02066 f^{2/3} \Big(\frac{\ln \frac{R_{\rm peb}}{R_0}}{\ln 10^4}\Big)^{-1} \Big(\frac{T_2}{150\,{\rm K}}\Big)^{-1} L_{*0}^{-2/7} M_{*0}^{8/7} \alpha_3^{-1} \dot{M}_{*8} \Big(\frac{Z_0}{0.01}\Big)^2 \Big(\frac{r_D}{\rm au}\Big)^{q_2 - 1} \Big(\frac{t}{t_{\rm pff}}\Big)^{\frac{2}{3}(q_2-1)} \Big(1 + \frac{t}{t_{\rm pff}}\Big)^{-\gamma_D} M_\oplus\,{\rm yr}^{-1} \quad (2.19)$$

where T_2 is the characteristic disk temperature, and R_0 and $R_{\rm peb}$ are the initial radii of dust particles and the pebbles when they start to migrate, respectively.

2.2.2 Planetesimal Accretion

According to the classical theory of Safronov (1969)[25], a solid protoplanet grows by accreting planetesimals ($\approx$ 1000 km sized objects). The growth mode of planetesimals is runaway growth. Protoplanets are formed through the runaway growth of planetesimals, and they continue to grow oligarchic. The relative growth rate in the runaway phase is given by[26]:

$$\frac{1}{m}\frac{dm}{dt} \propto m^{-\delta-2},\ {\rm with}\,\delta < -2 \quad (2.20)$$

where m is the mass of planetesimal.

The growth timescale for a protoplanet at $a > 2.7$ AU in a swarm of planetesimals is given by[26]:

$$T_{\rm grow} \simeq 9 \times 10^4 \Big(\frac{e}{h_M}\Big)^2 \Big(\frac{M}{0.0167\,M_\oplus}\Big)^{1/3} \Big(\frac{\Sigma_{\rm pl}}{4\,{\rm g\,cm^{-2}}}\Big)^{-1} \Big(\frac{a}{5\,{\rm AU}}\Big)^{1/2} {\rm yr} \quad (2.21)$$

where $h_M \simeq (M/3M_\odot)^{1/3}$ is reduced hills radius, $\Sigma_{\rm pl}$ is the surface mass density of planetesimals and M is the mass of protoplanet.

2.3 Orbital Evolution of Planets

The Orbital evolution of planets is determined by the gas disk-planet interactions. During formation, the planet cores migrate inwards due to the aerodynamical gas drag of pebbles and other particles. Type 1 migration occurs when a planet interacts with the gas in its immediate surroundings[18]. This interaction can cause the planet to lose angular momentum, causing it to spiral inward toward the star. In the simulations, the equation of motion incorporates planet-disc interactions based on dynamical friction, as proposed by Ida et al. (2020)[21].

$$\frac{d\vec{v}}{dt} = -\frac{v_k}{2\tau_a}\vec{e}_\theta - \frac{v_r}{\tau_e}\vec{e}_r - \frac{v_\theta - v_k}{\tau_e}\vec{e}_\theta - \frac{v_z}{\tau_i}\vec{e}_z \tag{2.22}$$

where, $\vec{v}$ is the planetary velocity evaluated at the instantaneous orbital radius r, with v_r, v_θ, and v_z being its polar coordinate components defined with the unit vectors $\vec{e}_r$, $\vec{e}_\theta$, and $\vec{e}_z$, respectively. Lastly, v_K is the Keplerian orbital speed evaluated at the instantaneous orbital radius r.

The evolution timescales for the semi-major axis, eccentricity, and inclination are expressed as follows:

$$\tau_a = -\frac{t_{\rm wave}}{2h_g^2}\left[\frac{\Gamma_L}{\Gamma_0}(1 - \frac{1}{\pi}\frac{\Gamma_L}{\Gamma_0}\sqrt{\hat{e}^2 + \hat{i}^2})^{-1} + \frac{\Gamma_C}{\Gamma_0}\exp(-\frac{\sqrt{\hat{e}^2 + \hat{i}^2}}{e_f})\right]^{-1} \tag{2.23}$$

$$\tau_e = \frac{t_{\rm wave}}{0.780}\left[1 + \frac{1}{15}(\hat{e}^2 + \hat{i}^2)^{3/2}\right] \tag{2.24}$$

$$\tau_i = \frac{t_{\rm wave}}{0.544}\left[1 + \frac{1}{21.5}(\hat{e}^2 + \hat{i}^2)^{3/2}\right] \tag{2.25}$$

where $h_g = H_g/a$ is the gas disc's aspect ratio, and eccentricities and inclinations scaled with h_g are defined as $\hat{e} = e/h_g$ and $\hat{i} = i/h_g$, respectively. Exponential factor $e_f = 0.01 + h_g/2$. Γ/Γ_0 0 represents a normalized torque, and the subscripts L and C respectively correspond to Lindblad and corotation torque. Last, $t_{\rm wave}$ is the characteristic time of wave induction in the disc, which propels the migration and is given by

$$t_{\rm wave} = \Big(\frac{M_*}{M_p}\Big)\Big(\frac{M_*}{\Sigma_g a^2}\Big)h_g^4\Omega_{k,a}^{-1}\,{\rm yr} \tag{2.26}$$

where M_p and M_* are planetary and stellar masses, respectively, Σ_g is the gas disc's surface mass density, and $\Omega_{K,a}$ are the Keplerian orbital speed and the corresponding angular speed evaluated at the semi-major axis.

Methods

The orbital evolution of a planetary system belongs to a classical physics problem: the N-body problem. To study the formation of giant planets and their evolution, N-body simulations were run, as further described in 3.1. In Section 3.2, the software packages used to run the simulations are described. The variables in the disk parameter space and the initial conditions used are described in the consecutive sections.

3.1 N-body Simulations

An N-body simulation is a computational method that approximates the motion of particles, typically particles that interact with each other through physical forces. Specifically, gravitational N-body simulations are numerical solutions for the equations of motion of N particles that interact gravitationally[27]. The algorithm[27] for N-body simulations involves calculating the force acting on a given particle from all other particles in the system. This calculation is done at regular intervals or time steps, updating each particle's position and other attributes based on the net force acting upon it. In systems where gravity is the dominant force, the simulation can predict the movements and trajectories of particles over time by solving the equation of motion numerically, given the initial positions, velocities, and masses of the particles. However, the computational complexity of the simulation grows as the square of the number of particles (N^2), limiting the maximum value of N due to the time required to calculate the forces.

The underlying symmetry of the N-body equation of motion can be represented in the Hamiltonian formulation[28]. A symplectic integrator (SI)[29] is a numerical integration scheme that preserves the potential energy of a Hamiltonian system. Kepler solver[29] is an analytical method used to solve the two-body problem, specifically Kepler's Equation over the entire range of elliptic motion. It predicts the orbit of a planet and its motion over time.

3.2 Software Packages

3.2.1 SWIFT SyMBA

SWIFT follows the long-term dynamical evolution of a swarm of test particles in the solar system. The SWIFT subroutine package written by H. Levison and M. Duncan[30] is designed to integrate a set of mutually gravitationally interacting bodies with a group of test particles that feel the gravitational influence of the massive bodies but do not affect each other or the massive bodies. SyMBA is an extension of SWIFT which can symplectically integrate a full N-body system, including close approaches between the massive bodies. SwiftVis[31] is a tool for analyzing and visualizing data, originally designed to focus on Swift data processing.

3.2.2 GENGA

GENGA (Gravitational Encounters with GPU Acceleration)[32] is a hybrid symplectic N-body integrator designed explicitly for the integration of planet and planetesimal dynamics during the later stages of planet formation and for conducting stability analyses of planetary systems. GENGA employs a hybrid symplectic integrator that incorporates maneuvering change-over functions to effectively handle close encounters to ensure long-term integration of planetary systems with high accuracy in energy conservation.

Table 3.1: List of tested parameters and their range of values

No.	Parameter	Symbol	Unit	Literature Range	Tested values
1	Gas disk diffusion timescale	$t_{\rm diff}$	Years	10^{5-7}	10^5, 5×10^5, 10^6, 10^7
2	Accretion due to disk turbulence	$\alpha_{\rm turb}$	-	$10^{-(3-5)}$	10^{-3}, 10^{-4}, 10^{-5}
3	Gas accretion coefficients	b, c	Yr, -	10^{6-9}, $2.5-3.5$	$(10^8, 10^9), (2, 3, 4)$
4	Pebble accretion efficiency prescription	peb_flg	-	-	-
5	Sticking efficiency	f	-	0 - 1	0.1,0.5,0.75,1
6	Disk inner and outer edge	$r_{\rm in}, r_{\rm out}$	AU	1-5, 100-500	5, (100,500)
7	Mass of gas disk	$M_{\rm disk,0}$	$M_\oplus$	0.01-0.1	0.05,0.1
8	Total mass in planetesimals	$M_{\rm tot}$	$M_\oplus$	0.01-4	(0.5,1,4)
9	Slope of initial planetesimal size distibution	β	-	(2.5,4.5)	2.5,4.5
10	No. of self-gravitating particles	$\#sg$	Thousand (K)	-	(1,1.5,2.4,3.2,4.5)

3.3 Parameter Space

The parameter space required to generate the desired gas disk and initial conditions is extensive. The number of parameters utilized in this study is contingent upon the specific goals of the simulations, and their respective values will be explicated in the results section. Herein, the parameters of central importance to this research will be defined, and their respective significance will be expounded upon.

The following table (3.1) lists the tested parameters:

1. **Disk Diffusion Timescale** $(t_{\rm diff})$
   It is the time required for the gas to completely diffuse out of the circumstellar disk. It is estimated to be around a few million years or less (Eq. 2.11).

2. **Accretion Strength and Disk Turbulence** (α)
   In this work, prescription given by Ida et al. (2018)[20] is followed. Two different α values were adopted: one representing the disc accretion driven by the mass loss due to the magnetic disc wind $\alpha_{\rm acc}$ (Eq. 2.2), and the other representing the local disc turbulence $\alpha_{\rm turb}$ (Eq. 2.13). The former is computed self-consistently in our N-body code, while the second is an input parameter.

3. **Gas Accretion Parameters** $(b$ **and** $c)$
   These parameters affect the growth rate of the gas envelope around the planet core (Eq. 2.10).

4. **Pebble Accretion Efficiency**(peb_flg)

   Two pebble accretion efficiency prescriptions were tested, one given by Ida et al. (2018)[20] (Eq. 2.13) and Ormel et al. (2018)[22] (Eq. 2.14). Both these have a varying effect on the result of the simulation.

5. **Planetesimal Accretion**

   A solid protoplanet growth by accreting planetesimals ($\sim$ 1000 km sized objects) (Eq. 2.20). I used GENGA to run these simulations.

6. **Pebble Sticking Efficiency** (f)

   The pebbles are assumed to form from dust coagulation in a front sweeping outward through the disc[24]. The dust coagulation does not have to be perfectly efficient because dust grains can bounce rather than stick. The parameter f gives the efficiency for pebble growth due to dust grain coagulation in the front.

7. **Disk Taper**

   The disk taper is switched on and off by commenting out the exponential decrease factor from the pebble mass flux equation. When the disk taper is "on," from Equation 2.19, we see that the pebble flux at the outer edge of the pebble formation front decreases exponentially. Consequently, there are not many pebbles for accretion. When the disk taper is "off," the last argument in Equation 2.19 is commented out. Hence, there's no exponential decrease in pebble flux, and the embryos accrete enough pebbles to form giant planet cores.

8. **Disk Inner and Outer Edge**

   The inner edge defines the distance below which $(r < r_i)$ the test particles are lost to the Sun. The outer edge defines the radius after which $(r > r_o)$ the test particle is scattered out of the system.

9. **Mass of Gas disk** (m_{disk})

   The gas disk's "initial mass" pertains solely to the gas component and does not include contributions from pebble disks or the masses of planetesimals or embryos. The temporal changes in this mass are governed by the surface mass density and the mass flux from the star.

10. **Total initial mass of planetesimals**

    The total initial mass of planetesimals is a pivotal constraint in determining the initial size distribution of the planetesimal disk, alongside various other factors. This measure excludes the masses of the pebble and gas disks. As time progresses, the evolution of this mass occurs through the accretion of pebbles and the formation of planet cores and embryos.

11. **Self-Gravitating planetesimals and** m_{tiny}

    Particles that can accrete onto one another in conjunction with pebbles are referred to as self-gravitating particles. The number of such particles is a function of the available computational resources and time constraints. Ideally, all the particles would exhibit self-gravitational effects, but this would prove to be computationally demanding. Consequently, a value of m_{tiny} is arbitrarily established; only planetesimals exceeding this threshold will exhibit self-gravitational behavior. In practice, most of the planetesimals were self-gravitating.

3.4 Generating Initial Conditions

A total of 180 simulations featuring two-planet cores, 730 simulations featuring multiple-embryo cores, and over 480 (and more still running) production simulations featuring planetesimals were executed to assess the process of pebble accretion, alongside 20 additional simulations to evaluate planetesimal (core) accretion. In each simulation, a Sun-like star was assumed, and the disc's inner boundary was fixed at 5 AU. Every core was randomly assigned an initial eccentricity within the range of $e = [0, 0.01]$, an associated inclination of $i = 0.5e$ radians, and randomized phase angles. Additionally, planets were designated as ”removed” once their distance from the star exceeded 100 AU.

3.4.1 Pebble Accretion Simulations

Initial conditions comprise of

(a) The mass, radius, and density of the gas disk at t=0. Additionally, other values pertaining to the gas disk, as mentioned in the above section, were specified in the input files. The dust-to-gas ratio was set to 0.01.

(b) Planetesimals, embryo cores, and planet cores that were enveloped within the gaseous disk were produced through the utilization of a FORTRAN code in conjunction with pre-existing subroutines. The following equations governed the orbital elements (radius, eccentricity, semi-major axis, inclination, etc.). A migration trap (equivalent to a pressure bump in the gas disk) was set at 5 AU for large planets to prevent migration into the Sun and avoid using very short time steps.

The mass-radius relationship for embryos and planet cores that we use here is given by Seager et al. (2007)[33]. The following equation is satisfied by cold terrestrial planets $M < 20M_{\oplus}$ of all compositions.

$$\log\Big(\frac{R}{3.3\,R_{\oplus}}\Big) = k_1 + \frac{1}{3}\log\Big(\frac{M}{5.5\,M_{\oplus}}\Big) - k_2\Big(\frac{M}{5.5\,M_{\oplus}}\Big)^{k_3} \tag{3.1}$$

where M and R are the mass and radius of the planet, and where $k_1 = -0.20945$, $k_2 = 0.0804$, and $k_3 = -0.394$. This equation is true for the total mass of planets up to $M_p \approx 20M_{\oplus}$. Seager et al. (2007)[33] convincingly tested the same equation for gas giants with fixed core masses of 5, 10, 20, 50, and 100 $M_{\oplus}$.

The maximum radius of planetesimals was set to 2000 km. Consequently, the maximum mass of planetesimals in the initial distribution is given by the equation[9]:

$$M_{\rm pltms,init} \simeq 13.8M_{\oplus}\Big(1 + \frac{\mathcal{S}}{\alpha_{\rm turb}}\Big)^{-3/2} L_{*0}^{3/7} M_{*0}^{-5/7}\Big(\frac{r}{1\,{\rm au}}\Big)^{6/7} \tag{3.2}$$

where $\mathcal{S}$ is the Stokes number and $\alpha_{\rm turb}$ is the accretion strength due to turbulence.

The slope of the initial size distribution was set in radial distribution and not mass *(slope for mass dist. is approx. three times in a log-log plot)*. Both shallow and steep size distributions were tested. The total mass of the planetesimal disk and the minimum and maximum radius of the planetesimals were kept as variable parameters. The maximum radius was set such that the resulting planetesimals are smaller than Mars's mass cores. The radii are generated from a random number as

$$r_{\mathrm{pltms}} = r_{\mathrm{min}} \zeta^{-1/\beta} \tag{3.3}$$

where ζ is a random number from an uniform distribution between $(0, 1)$ and β is the size-frequency distribution slope. The other orbital elements (semi-major axis, eccentricity, inclination, the longitude of the node, the argument of perihelion, and mean anomaly) are uniformly generated with their appropriate multiplicative factors and limits.

However, due to the above-mentioned constraints, the initial distribution of planetesimals was not a direct power law but a truncated Pareto distribution.

Explanation of the Truncated Pareto Distribution[34]:

Let x be a random variable taking values in the interval $[a; \infty], a > 0$. Then the Pareto distribution function has a probability density function (PDF) given by

$$f(x; a; c) = ca^c x^{-(c+1)} \,\mathrm{with}\, c > 0, \tag{3.4}$$

Both the cumulative distribution, $P(X > x)$, also called the survival function, and the probability density function will give us a straight line on a log-log plot (linear fit on the plot 3.1) but their slopes differ by 1. The survival function is given by

$$P(X > x) = a^c x^{-c} \,\mathrm{with}\, c > 0, \tag{3.5}$$

A truncated Pareto random variable is defined in the interval $[a; b]$, and the corresponding PDF is

$$f_T(x; a; b; c) = \frac{ca^c x^{-(c+1)}}{1 - (\frac{a}{b})^c} \tag{3.6}$$

On a log-log plot, the distribution function $P(X > x)$ for this exhibits an almost linear trend, with a sharp drop when $x \to b$.

$$P(X > x) = \frac{1 - a^c x^{-c}}{1 - (\frac{a}{b})^c} \tag{3.7}$$

The above discussion is illustrated in the following figure for the initial size-frequency distribution of planetesimals.

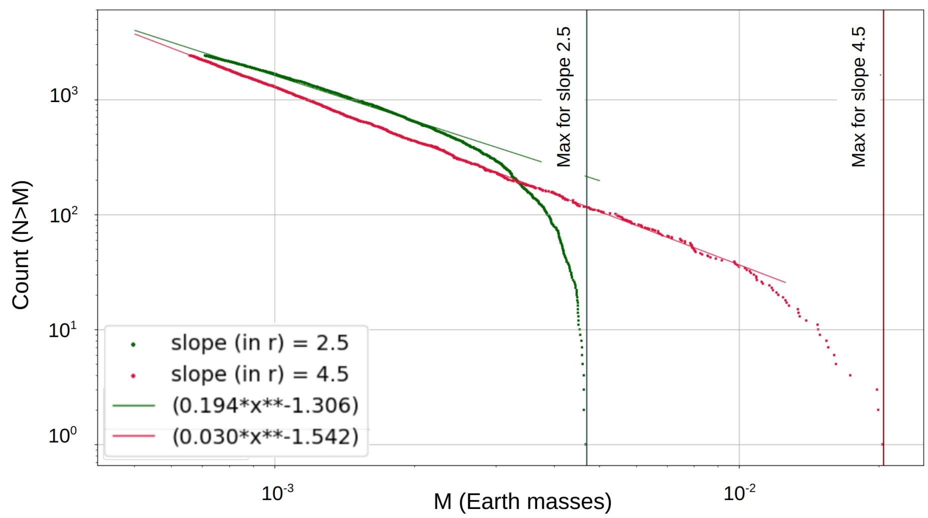

Figure 3.1: Initial size distribution for radial distribution with slope $\beta = 2.5$ (green) and 4.5 (red). Both data sets follow a truncated Pareto distribution, as expected. The slope for the initial size distribution set to $\beta = 2.5$ in the graph is 3.6. This is a consequence of truncated Pareto distribution on a fairly narrow range.

I have a fixed number of planetesimals and total mass while generating planetesimals, with the radius changing. Since $\beta = 4.5$ is steeper, and their maximum radius was fixed to 2000 km, to keep the number of bodies the same, in the distribution, I get heavier bodies for the steeper slope than $\beta = 2.5$.

3.4.2 Core Accretion Simulations

With improved computational power, availability of GPU cores, and a competent GENGA code[32], I decided to test the Core Accretion theory[25]. The runs were done with different planetesimal populations with varying mass, size distributions, and numbers, between 5.5 AU and 30 AU. These simulations were run for 10 million yrs and concentrated only on the formation of giant planet cores, not the consecutive gas accretion. The total mass of planetesimals was fixed to 30 or 40 $M_{\oplus}$, and their maximum radius was fixed to 2000 km. We varied the number of planetesimals from 10K to 45K. The disk's inner edge was set to 3.5 AU and the outer edge to 100 AU. The Core Isolation Mass *(the mass at which the growth rate decreases rapidly)* is set to approximately $2M_{\odot}$.

Results

In the preceding chapter, I explicated the parameters within the selected parameter space. The optimal values of these parameters were chosen to achieve the most accurate replication of our objective. This chapter will focus on the simulations conducted, their respective outcomes, and the underlying justification for selecting the final set of parameters for each simulation.

4.1 Simulations with Pebble Accretion onto Two Planet Cores

The objective of these computer simulations was to create giant planets in a gaseous disk using two planet cores. They initiated with Jupiter ($0.01 M_\oplus$) and Mars ($0.001 M_\oplus$) cores at 5.6 AU and 1.5 AU, respectively, in order to determine three important disk parameters: $t_{\rm diff}$, $\alpha_{\rm turb}$, and gas accretion parameters `b` and `c`. Both Ida and Ormel pebble accretion models ($\rm peb\_flg = 0, 1$) were tested. To avoid the cores from experiencing type I migration during the accretion process, migration was disabled. The simulations were conducted for a period of 5 Myrs to observe the final planetary evolution. The results for these simulation sets are summarized in the following table.

In the table 4.1, we list the values for the given parameters that we tested, and below that, we list the best-fit parameters:

Table 4.1: Disk Parameters for Two Planet Simulations

S.No.	Parameter	Values of Par.	Remarks
1	t_{diff}	10^5	Gas diffused too quickly for the planets to accrete
		10^6	Forming Jupiter-sized planets
		10^7	Gas stays for long period; not very reasonable
2	α_{turb}	10^{-5}	Planets did not accrete a lot
		10^{-4}	Forming Jupiter-sized planets
		10^{-3}	There is no physical explanation for a high accretion strength due to turbulence
3	Gas Acc. Par. b	10^8	Giving positive results
		10^9	Giving negative results
	c	2.0	Gives negative results for the Ida prescription of pebble accretion
		3.0	Giving positive results
		4.0	Forms very heavy gas giants that are not seen in solar system
4	peb_flg	0	Forming gas giants and Earth-sized cores across the disk
		1	Forming gas giants near the inner edge of the disk

$$t_{\text{diff}} = 1\,\text{Myr} \quad b = 10^8\text{yr}$$
$$\alpha_{\text{turb}} = 10^{-4} \quad c = 3$$

Figure 4.1 indicates the mass and semi-major axis of planets formed with the chosen parameters.

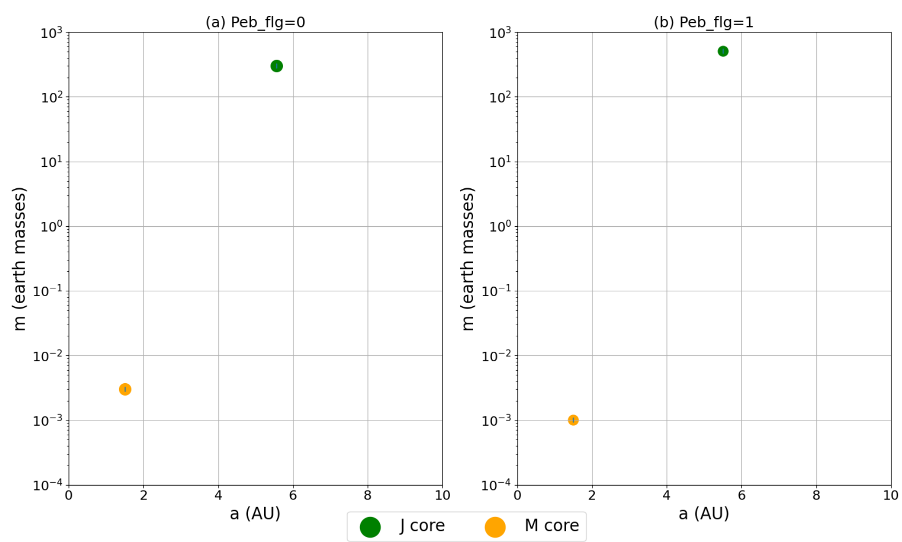

Figure 4.1: Result at the end of 5 Myrs. For both the pebble accretion prescriptions, we can see that Jupiter core (green) grows above 300 Earth masses. The Mars core (orange) does not grow because the pebble migration is shut off by the growing Jupiter.

Table 4.2: Disk Parameters for Multiple Embryo core Simulations

S.No.	Parameter	Values of Par.	Remarks
1	t_{diff}	10^6	Forming Jupiter-sized planets
		0.5×10^6	Decreased the diffusion time of gas to constrain growth of gas giants; produces gas planets in desired mass range.
2	α_{turb}	10^{-4}	Decided in above section
3	Gas acc. par. b	10^8	Decided in above section
		10^9	Small test was done with slower accretion rate to see if planets accrete as desired. It didn't.
4	c	3.0	Decided in above section
5	peb_flg	0	Forming gas giants and earth-sized cores across the disk
		1	Forming gas giants near the inner edge of the disk
6	N	7	Accretion was as expected
		14	Accretion was as expected
7	r_{out}	100	Reasonable value to obtain gas giants
		500	For same disk mass, disk surface density reduces significantly and does not produce giant planets.
8	m_{disk}	0.05	Reasonable value to obtain gas giants
		0.1	High disk mass resulted in overly massive planets
9	t_{pff}	on	Giving negative results
		off	Giving positive results
10	f	1	Ideal Value
		0.1	Giving negative results
		0.5	Giving positive results

4.2 Simulations with Pebble Accretion onto multiple embryo cores

The subsequent stage involved examining whether the parameters outlined in 4.2 led to the formation of gas giants via pebble accretion onto embryos in the protoplanetary disk. The simulations were once again conducted for both accretion efficiency models. Lunar-sized embryos, each 0.01 $M_{\oplus}$, were evenly distributed between 5 AU and 30 AU and permitted to undergo migration while undergoing pebble accretion. The inner boundary of the disk was established at 5 AU in order to prevent further inward migration. The growth pattern of planets was consistent with an inside-out process, as pebbles were drawn toward the Sun due to inward drift. The subsequent table provides an overview of the parameter range and corresponding outcomes.

As is clear from the above table 4.2, I selected the following values for the given parameters that yielded the best outcome:

$$
\begin{array}{lll}
t_{\text{diff}} = 0.5\,\text{Myr} & b = 100\,\text{Myr} & c = 3.0 \\
\alpha_{\text{turb}} = 10^{-4} & \text{peb\_flg} \ = \ 1 & f = 1, 0.5 \\
\text{Disk taper } = \text{off} & m_{\text{disk}} = 0.05 M_{\oplus} & r_{\text{D}} = 100\,\text{AU}
\end{array}
$$

With this value of t_{diff} the accretion rate onto the star becomes approximately $10^{-9}\ M_{\odot}$ yr^{-1} after about 5 Myr of evolution. At this accretion rate, photo-evaporation of the disc may be set in Matsumura et al. (2021)[9], and the disc density decreases rapidly. As such, I ran our production simulations for 5 Myr. Figure 4.2 indicates the mass, semi-major axis, and eccentricity of planets formed with the chosen parameters.

(a)

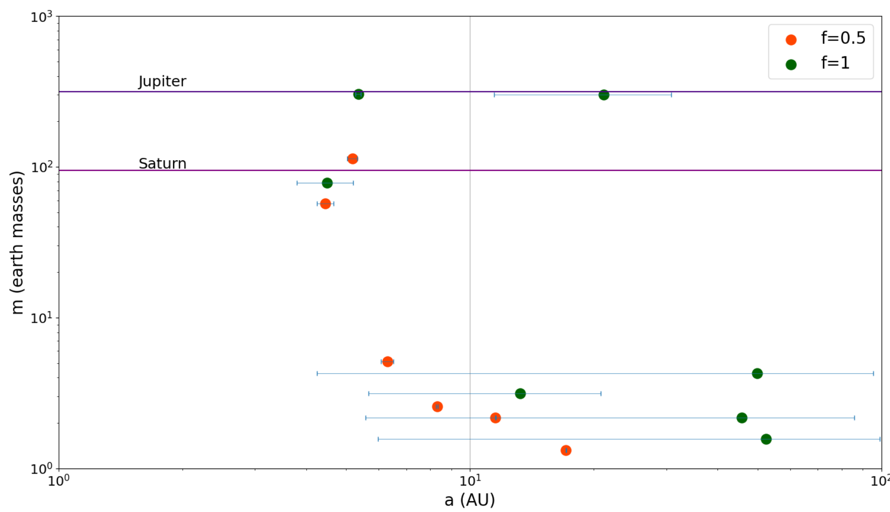

Figure 4.2: Simulations with Pebble Accretion onto Embryo Cores: With (a)7 cores, gas giants are formed. With $f = 1$ (green), both Jupiter and Saturn mass planets are formed, while with $f = 0.5$ (orange), only Saturn is formed. Error bars are a measure of eccentricities.

(b)

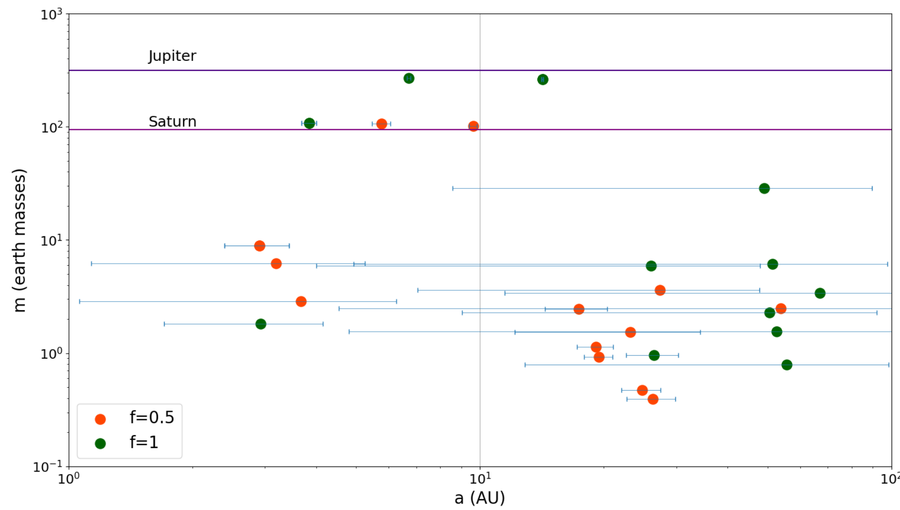

Figure 4.2: Simulations with Pebble Accretion onto Embryo Cores: With (b) 14 cores, gas giants are formed. With $f = 1$ (green), both Jupiter and Saturn mass planets are formed, while with $f = 0.5$ (orange), only Saturn is formed. Error bars are a measure of eccentricities.

4.3 Production Simulations: Pebble Accretion onto Planetesimals

The previous simulations resulted in the production of eccentric giant planets. However, if the simulations were continued for over 5 Myrs, some of these gas giants could have been scattered out of the system, leaving only one or a few planets behind. This outcome conflicts with the observation of the solar system, which contains two gas planets (Jupiter and Saturn) with very low eccentricities.

To address this discrepancy, the introduction of planetesimals and pebbles into the system is hypothesized to dampen the eccentricities of the gas giants by decreasing their angular momentum while also growing their masses[8]. In this set of simulations, the focus was on generating the optimal population of planetesimals that can accrete to form both gas giants and icy planets. The simulation parameters were selected based on the variation of the total mass, size distribution, and total number. The planetesimals were located between 5 AU and 25 AU, and a few runs with $\mathrm{peb\_flg} = 0$ were conducted to evaluate their reproducibility in the new environment.

As a part of the Production Simulation study, over 400 runs were conducted using 30 different parameter combinations. All simulations were optimized for the formation of Saturn. The parameter space used and analyzed in these simulations is presented in the flowchart shown in Figure 4.3.

4.3.1 Pebble Accretion is sensitive to different parameters

I started with a detailed examination of individual parameters. This entails the comparison of the final mass (size) distribution functions, corresponding to various parameters, at the end of 5 Myrs.

The figures (Fig. 4.4) depict cumulative functions combined from the output of 15 simulations, comparing f, $\mathrm{peb\_flg}$, m_{tot}, slope β and N.. Nearly all of the representative data sets exhibit a probability of over 60% for the formation of Saturn-mass planets. However, subtle variations arise when analyzing each parameter individually. In particular, the $\mathrm{peb\_flg}$ parameter shows little variation, except when the sticking efficiency f is maximal. The number of planetesimals N and the initial size distribution of planetesimals β do not display significant differences in the formation of Saturn and heavier gas giants. As anticipated, an increase in the total mass of planetesimals m_{tot} leads to the formation of heavier planets. Notably, the probability of obtaining Saturn increases with higher sticking efficiencies f. The outcome seems to be most sensitive to the original planetesimal disk mass, m_{tot}, and sticking efficiency, f.

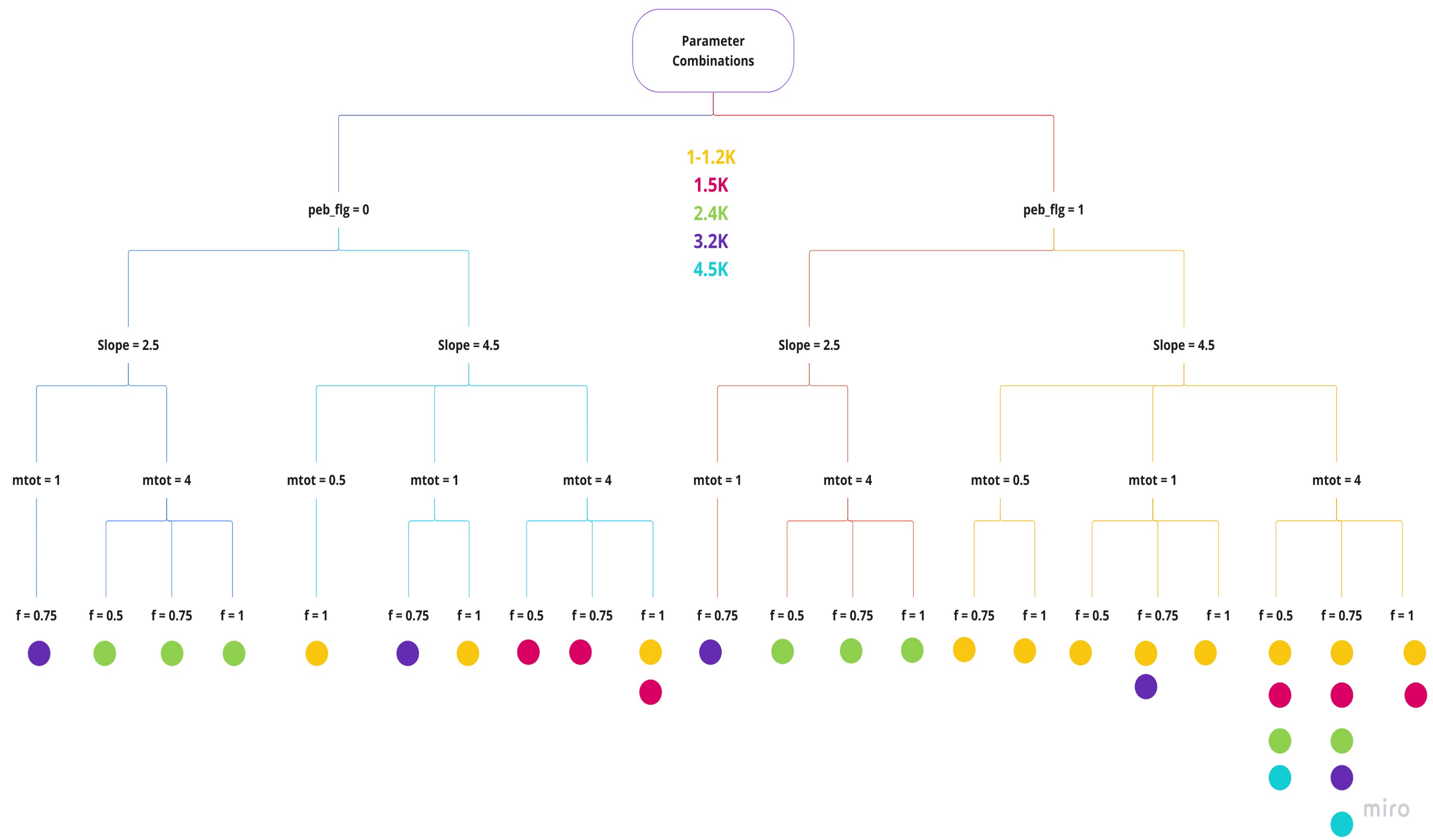

Figure 4.3: Parameter Combination for Production Simulations. Circles represent a set of 15 runs.

(a)

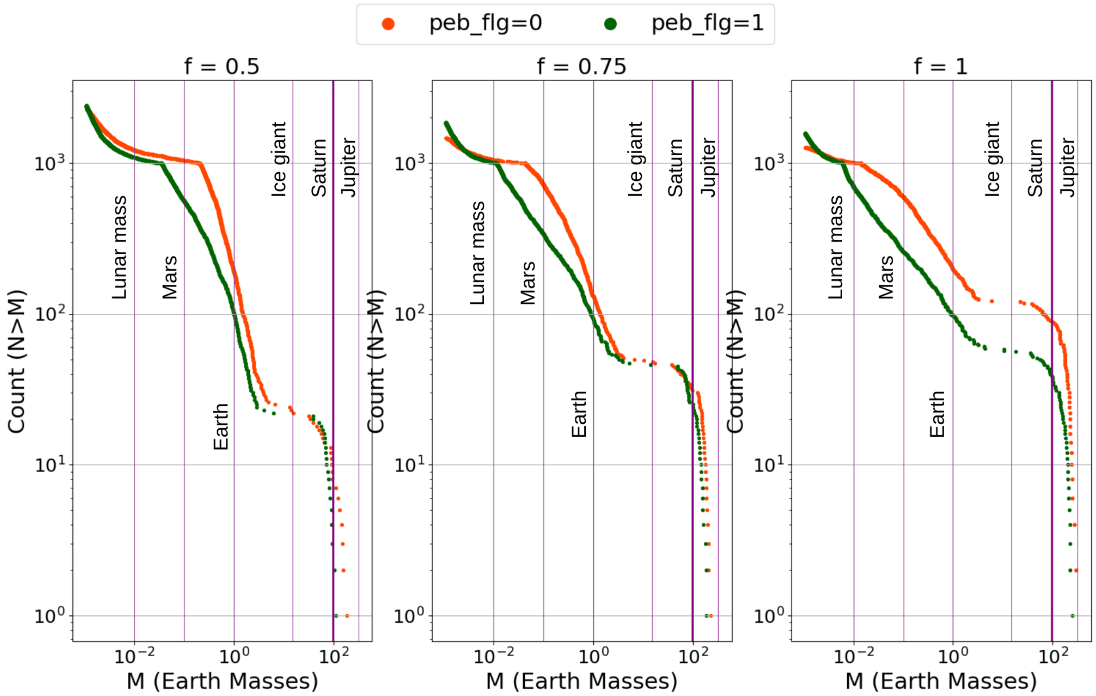

(b)

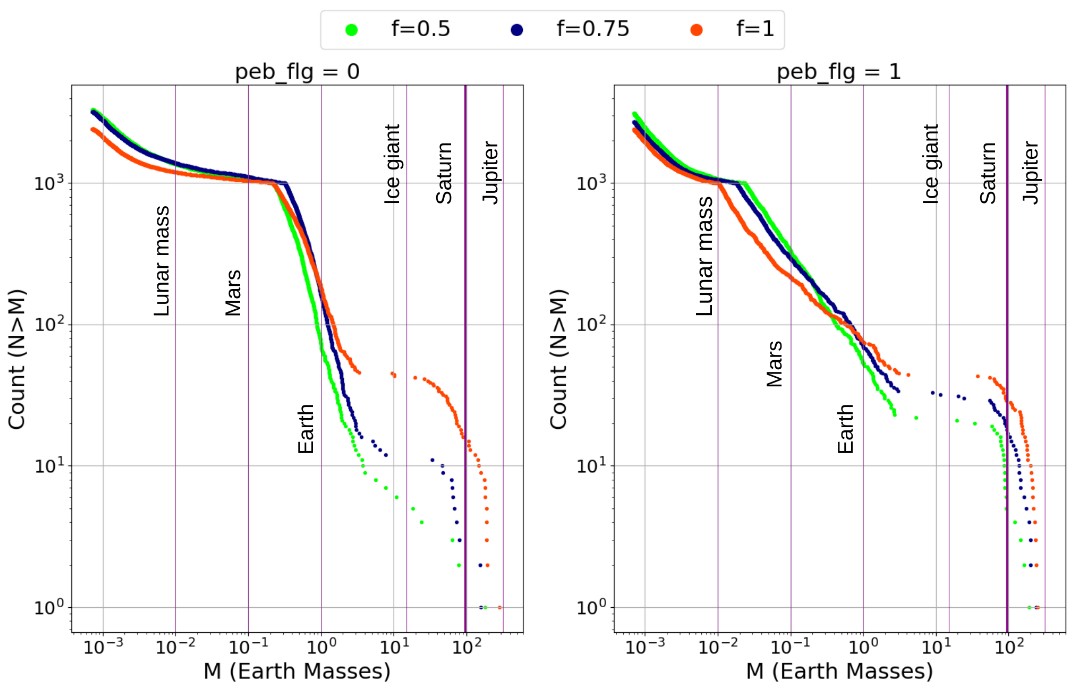

Figure 4.4: Final Size distributions of planetesimals and planet cores. The graphs give a comparison between (a) $\mathrm{peb\_flg}$ and f, and (b) f

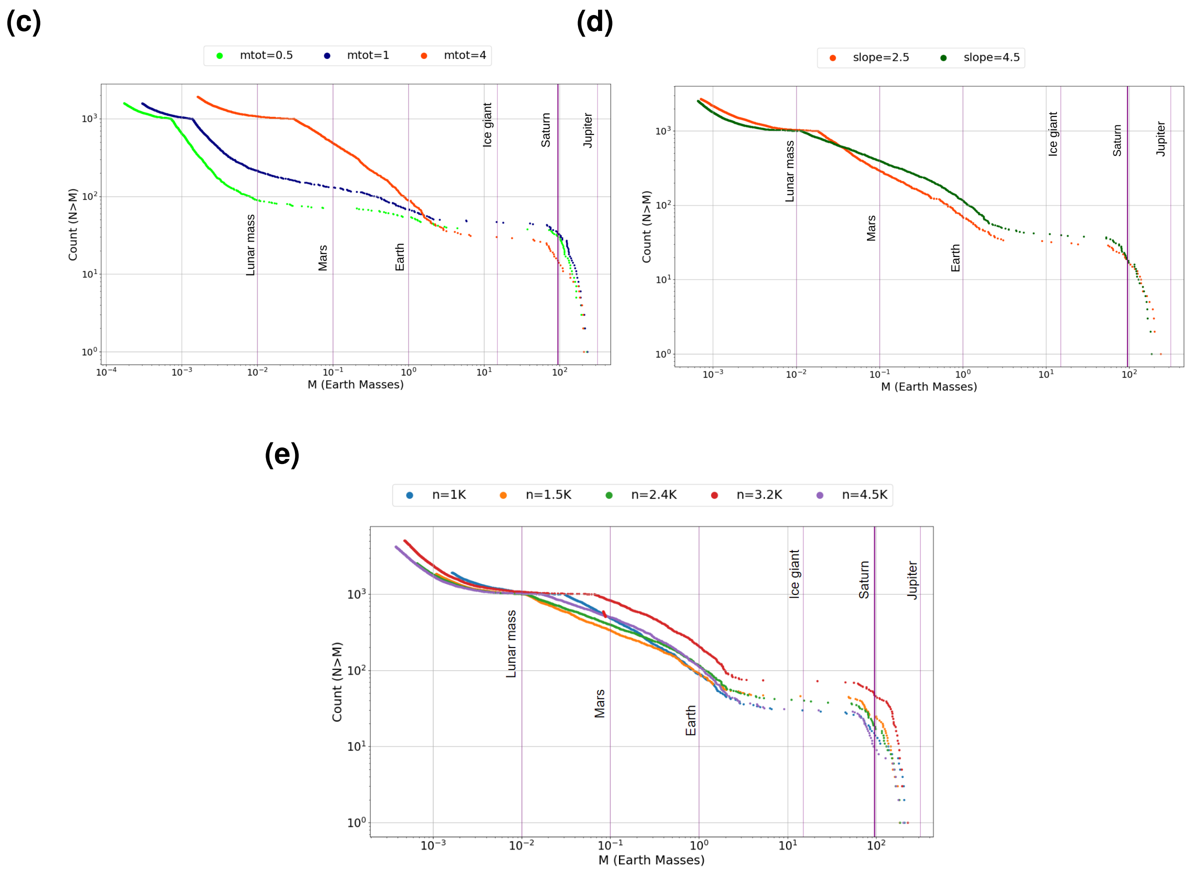

Figure 4.4: Final Size distributions of planetesimals and planet cores. The graphs give a comparison between (c) $m_{\rm tot}$ (d) β (e) N

4.3.2 Probability of forming Saturn

To determine the success rate of the formation of Saturn, probability distribution graphs were generated. While the simulations were designed specifically for attempting to form Saturn, the resulting figures demonstrate the formation distribution of Saturn, Jupiter, and ice giants analogs for all sets. The four variables analyzed include accretion efficiency ($\rm peb\_flg$), the slope of the initial planetesimal distribution (β), the total mass in planetesimals ($m_{\rm tot}$), and sticking efficiency (f). The *Frequency of occurrence* depicted in these graphs, refers to the $\#$ sets with *Planets per Run* (binned) value.

(a)

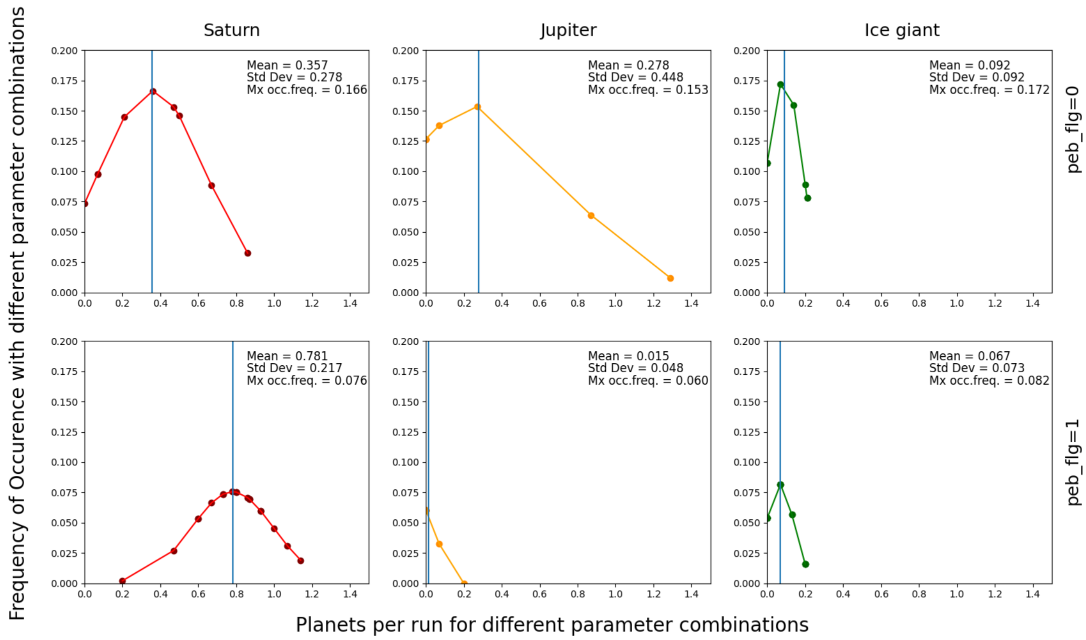

(b)

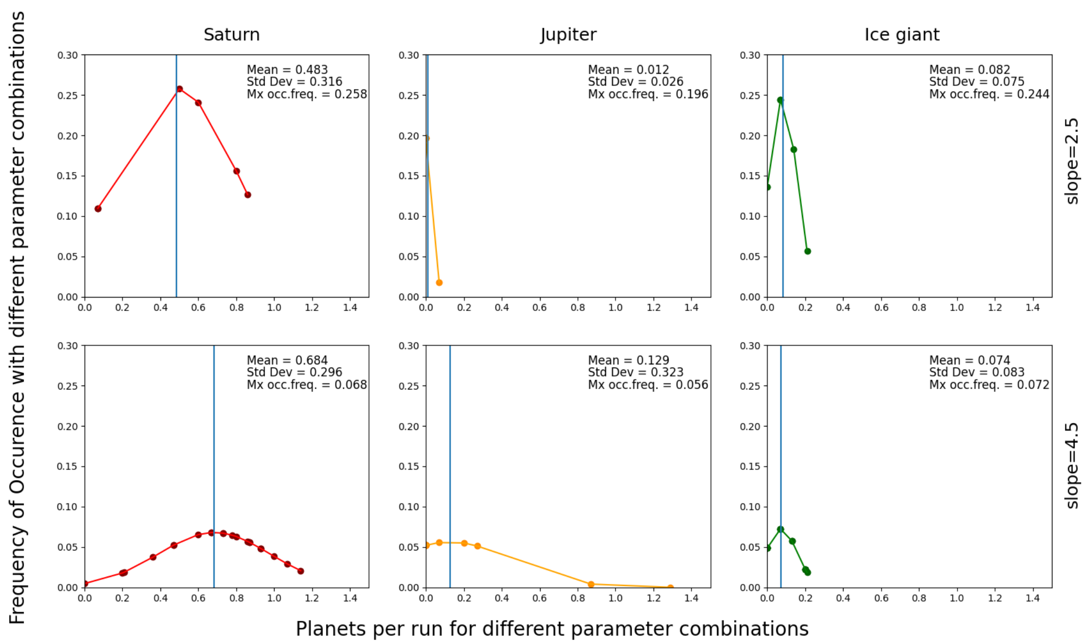

Figure 4.5: Frequency of occurrence vs probability of forming of planets: Cumulative distribution of all sets for (a) $\mathrm{peb\_flg}$ (b) β

(c)

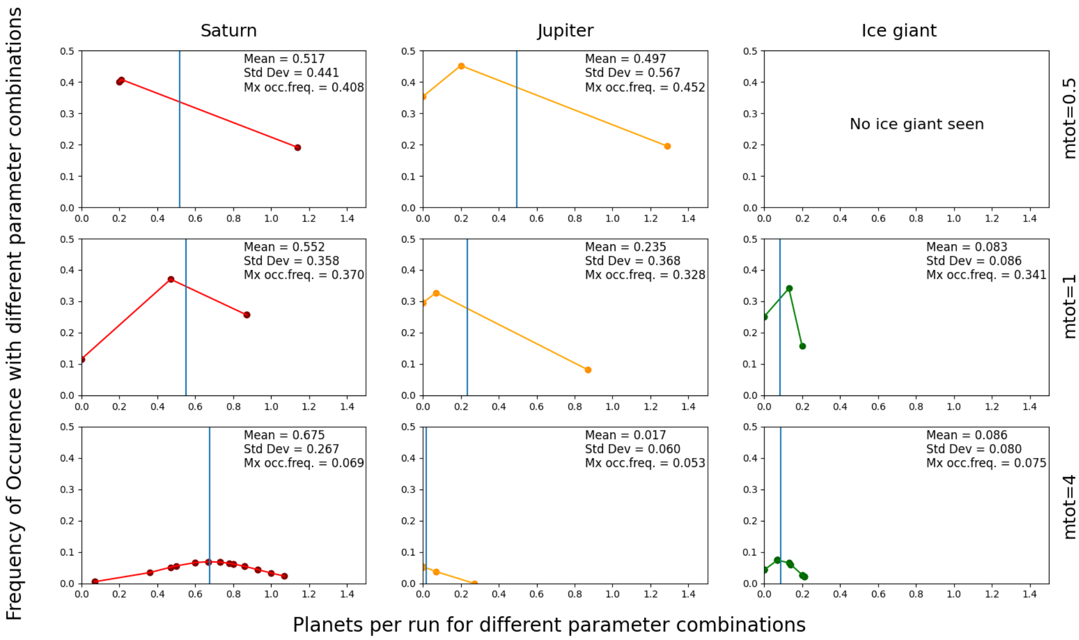

(d)

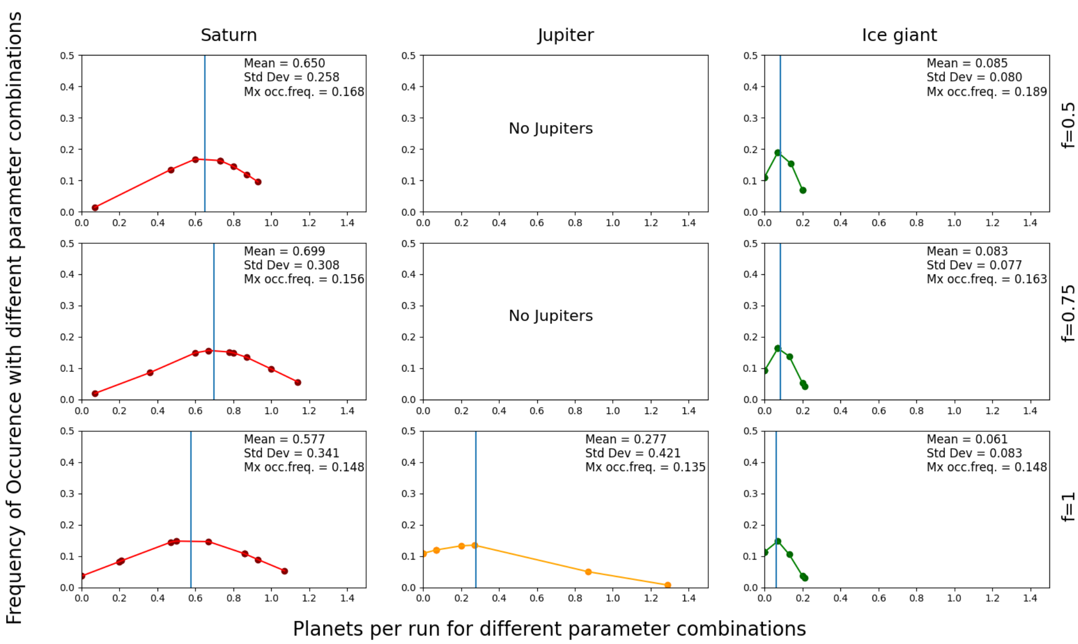

Figure 4.5: Frequency of occurrence vs probability of forming of planets: Cumulative distribution of all sets for (c) $m_{\rm tot}$, and (d) f.

The highest probability (refer x-axis of fig. 4.5) of forming Saturn is for the parameters: $\mathrm{peb\_flg} = 1$, $\beta = 4.5$, $m_{\mathrm{tot}} = 4$ and $f = 0.75$. However, I only form Jupiter analogs with reasonable probability when $\mathrm{peb\_flg} = 0$, but at the expense of forming Saturn analogs. Ice giant formation seems to be a low-probability occurrence for all combinations of parameters. It is not clear why the steeper slope produces better Jupiter analogs. The higher sticking efficiency produces more Jupiter analogs seems clear because accretion is generally faster than with higher sticking efficiency.

4.3.3 We do not get all three types of giant planets together

From the above two-fold analysis, I used the following two sets of combinations of input parameters to display the final orbital distribution of planets.

$$\begin{array}{lllll} \mathrm{peb\_flg} = 0 & f = 1 & m_{\mathrm{tot}} = 4 & \beta = 4.5 & N = 1.5K \\ \mathrm{peb\_flg} = 1 & f = 0.75 & m_{\mathrm{tot}} = 4 & \beta = 4.5 & N = 2.4K \end{array}$$

The following figure (Fig. 4.6) shows the final orbital element distribution for the above 2 sets.

(a)

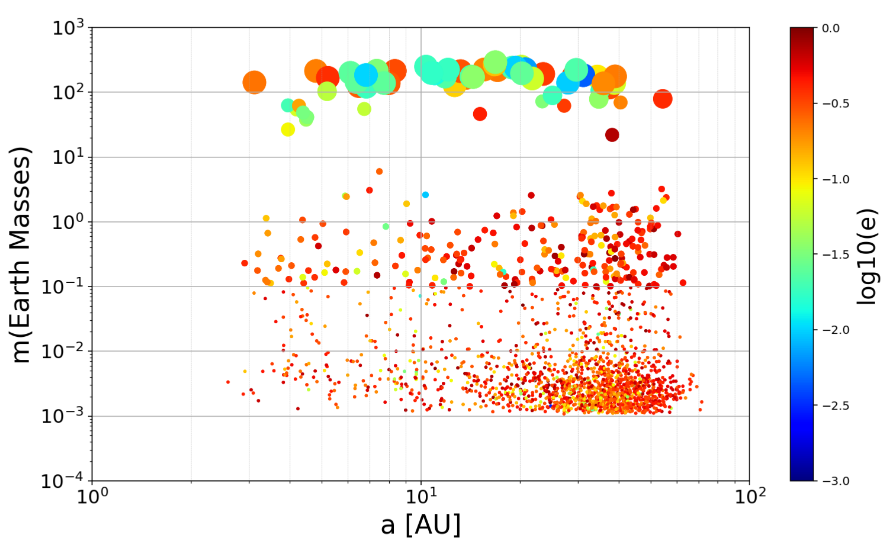

Figure 4.6: Log-log Mass vs. semi-major axis as a measure of eccentricity for the two selected sets. Initial Conditions: (a) $\mathrm{peb\_flg} = 0$, $f = 1$, $m_{\mathrm{tot}} = 4\ M_{\oplus}$, $\beta = 4.5$, $N = 1.5$K

(b)

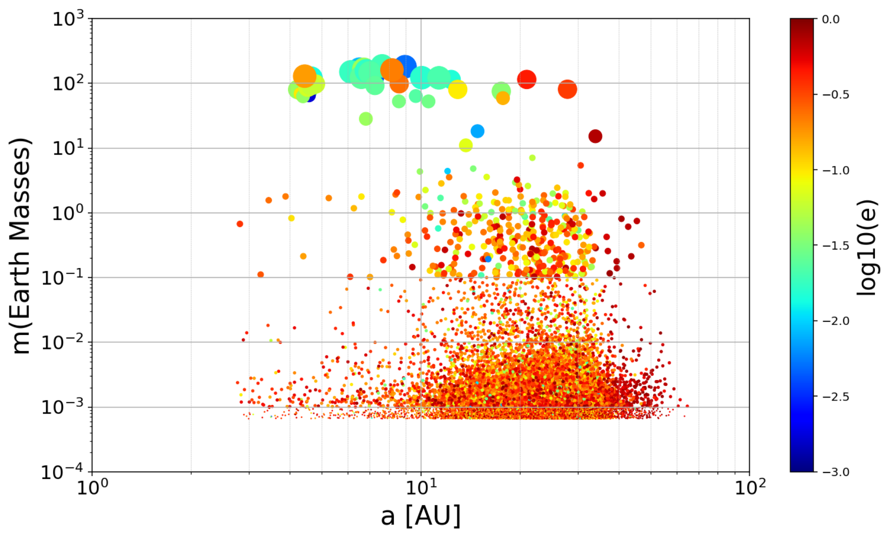

Figure 4.6: Log-log Mass vs. semi-major axis as a measure of eccentricity for the two selected sets. Initial Conditions:(b) $\mathrm{peb\_flg} = 1$, $f = 0.75$, $m_{\mathrm{tot}} = 4\ M_{\oplus}$, $\beta = 4.5$, $N = 2.4$K.

Although both groups contain a significant number of gas giants and ice giants with moderately high eccentricities, their combined distribution across all 15 trials is displayed in Fig. 4.6. In order to obtain a more accurate comprehension of the planet's distribution after 5 Myrs, I scrutinized each experiment separately, as illustrated in Figure 4.7.

(a)

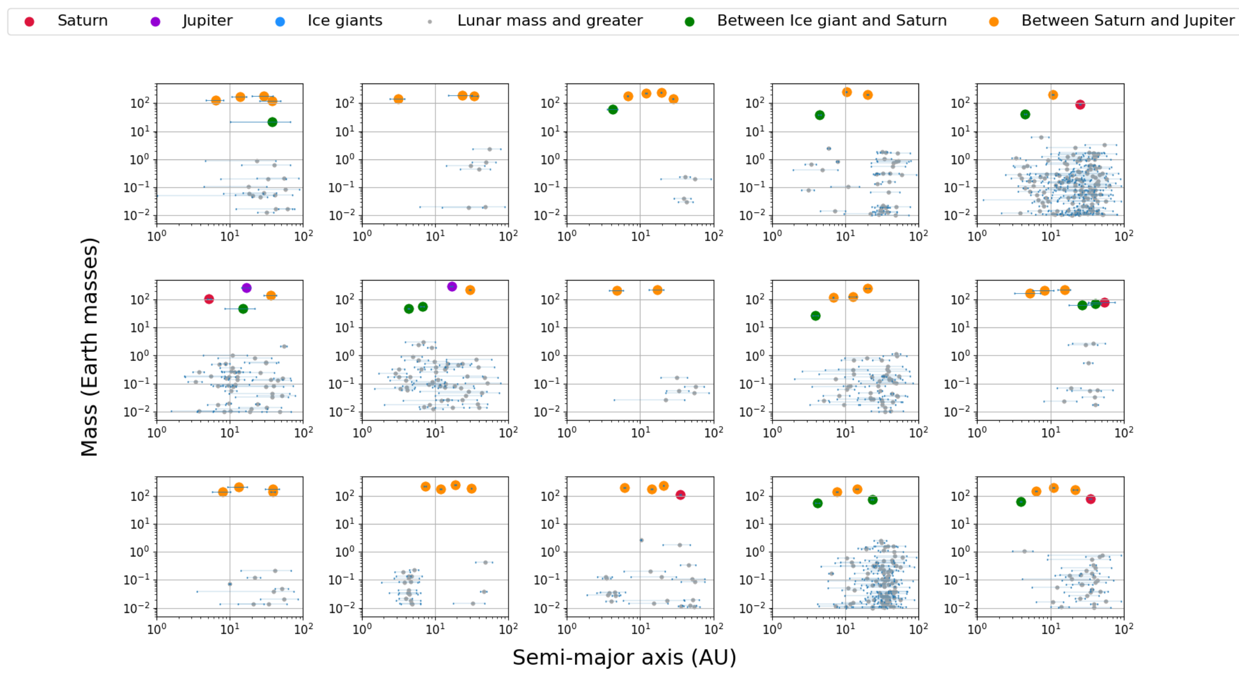

(b)

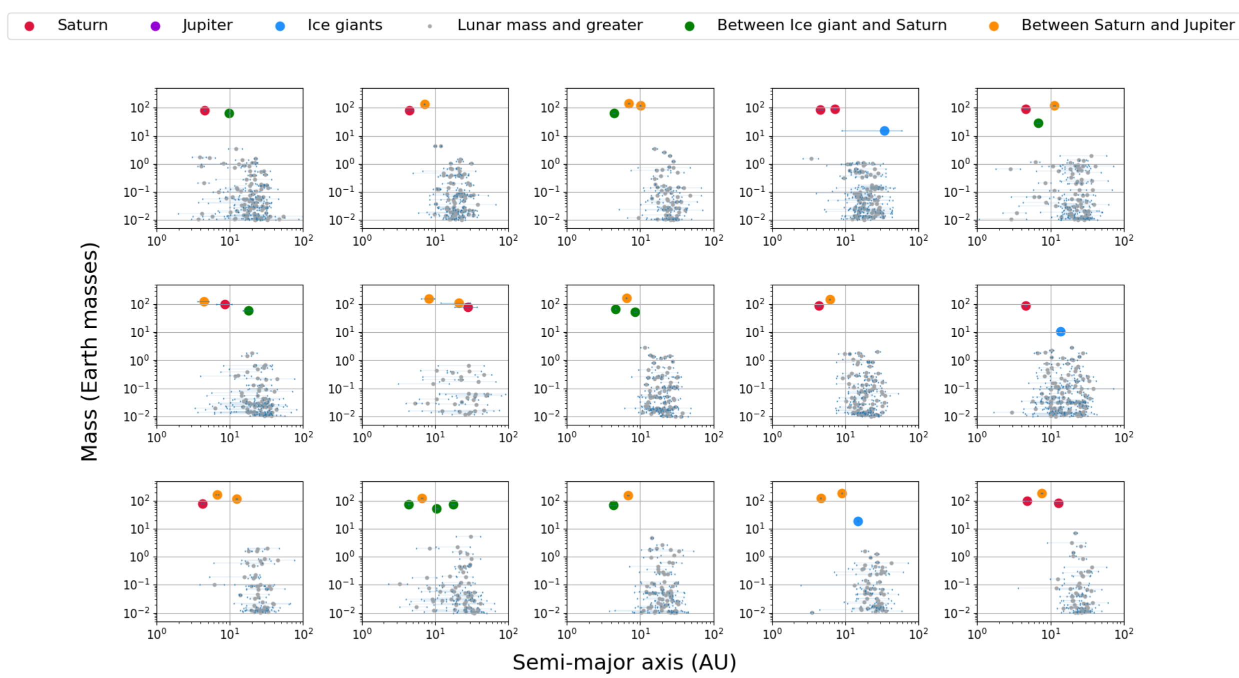

Figure 4.7: Mass vs semi-major axis distribution for each run of the two selected sets. Initial parameters: (a)$\mathrm{peb\_flg} = 0$, $f = 1$, $m_{\mathrm{tot}} = 4\ M_{\oplus}$, $\beta = 4.5$, $N = 1.5$K; (b)$\mathrm{peb\_flg} = 1$, $f = 0.75$, $m_{\mathrm{tot}} = 4\ M_{\oplus}$, $\beta = 4.5$, $N = 2.4$K. Mass ranges: Saturn (75,115) $M_{\oplus}$; Jupiter (254,380) $M_{\oplus}$; ice giants (10,20) $M_{\oplus}$.

It is evident that there are significant variations among all the trials in terms of the number of giant planets, their eccentricities, and the remaining mass of planetesimals. The runs with more planetesimals have a lower number of giant planets as well as they are less massive. Notably, we have **not** observed the formation of gas giants and ice giants in the same trial. The likelihood of obtaining Saturn with $\mathrm{peb\_flg} = 0$ and $f = 1$ is only 30%, with a greater chance of producing more massive gas giants. Conversely, the likelihood of obtaining Saturn with $\mathrm{peb\_flg} = 1$, $f = 0.75$ is more than 60%, with a considerable probability of generating ice giants.

4.4 Saturn Formation Time analysis

The successful formation of Saturn within a time frame of 5 Myrs has been demonstrated. In this section, I assess a theory outlined in the Introduction, which suggests that the Hf-W reset age of the Eagle Station Pallasite provides constraints on the time of Saturn's formation, estimated to be 2.8 Myrs. The final mass attained by a planet core with a mass of $75M_\oplus$ as a function of its formation time was examined, as illustrated in Figure 4.8 (a). The second graph, depicted in Figure 4.8 (b), presents a normal distribution fit for the time of Saturn's core formation. Both of these graphs were generated from the experiments that resulted in the formation of Saturn within 5 Myrs.

The figure (Fig. 4.8) reveals a linear relationship between the accretion time and the final mass achieved by a $75M_\oplus$ core, whereby earlier formation results in a more massive core at 5 Myrs. As such, it seems that the giant planets in the solar system could have formed sequentially. However, the formation time of Saturn has a wide distribution, with greater variability observed for $f = 0.5$ than for $f = 0.75$ or 1. The mean formation time of Saturn is presented in the lower panel as $\langle t_{\mathrm{Saturn}} \rangle = 3.09 \pm 1.33$ Myrs, which is in agreement with the Hf-W reset age of 2.8 ± 1.6 Myrs, lending support to our hypothesis. The standard deviation in the normal distribution is attributed to the differing influences of $\mathrm{peb\_flg}$, m_{tot}, and f.

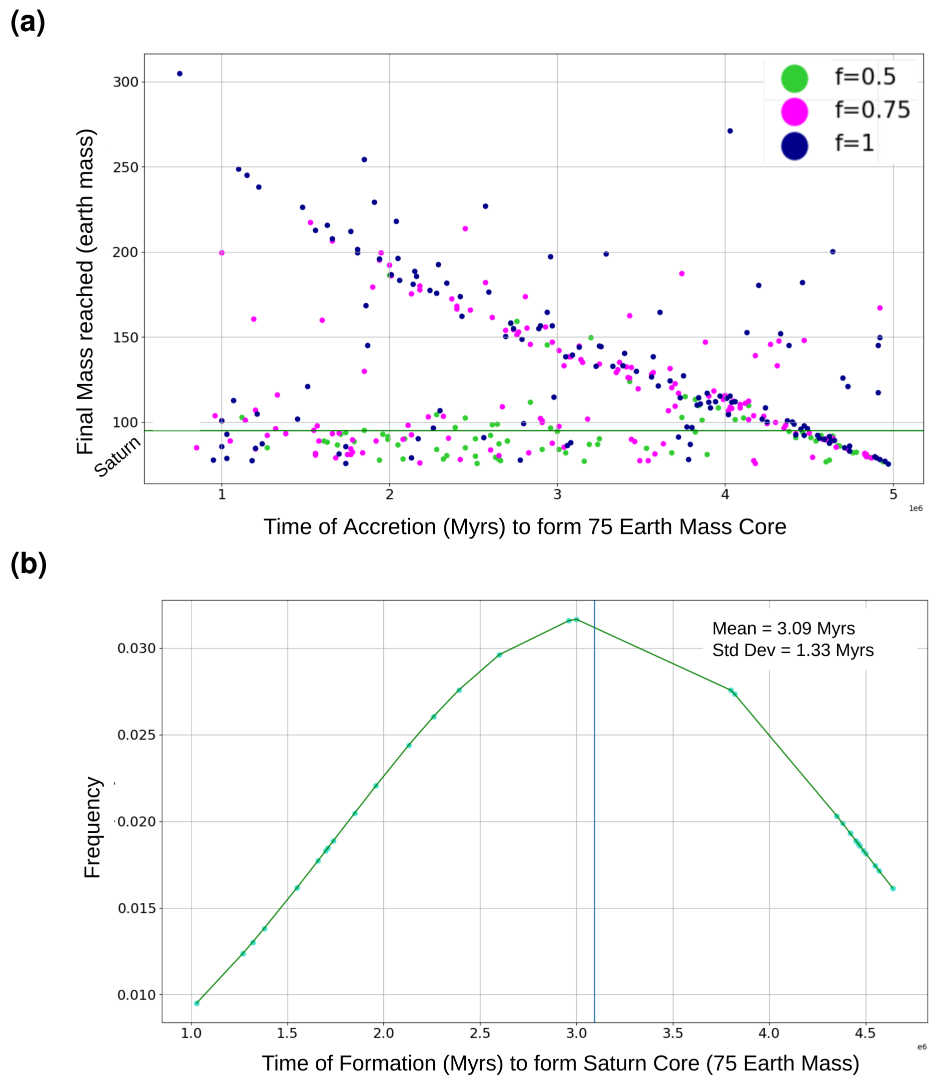

Figure 4.8: (a) Time of Accretion of $75M_{\oplus}$ core vs final mass reached. The distribution consists of data sets with different f. (b) Normal distribution of Formation time of Saturn. The data set is constrained for Saturn Masses between 90,100 $M_{\oplus}$.

To further validate the results of our simulations, I did the same analysis for the formation of an ice giant core (critical mass of $12M_{\oplus}$). Similar to the trend observed in Figure 4.8, a linear relationship is observed between the accretion time and final mass achieved by ice giants as well. Figure 4.9 indicates that Uranus and Neptune have very late formation times. The mean formation time of ice giants is $\langle t_{\rm ice} \rangle = 4.90 \pm 0.03$ Myrs. The uncertainty is low because the ice giants formed at the very end of the simulations.

(a)

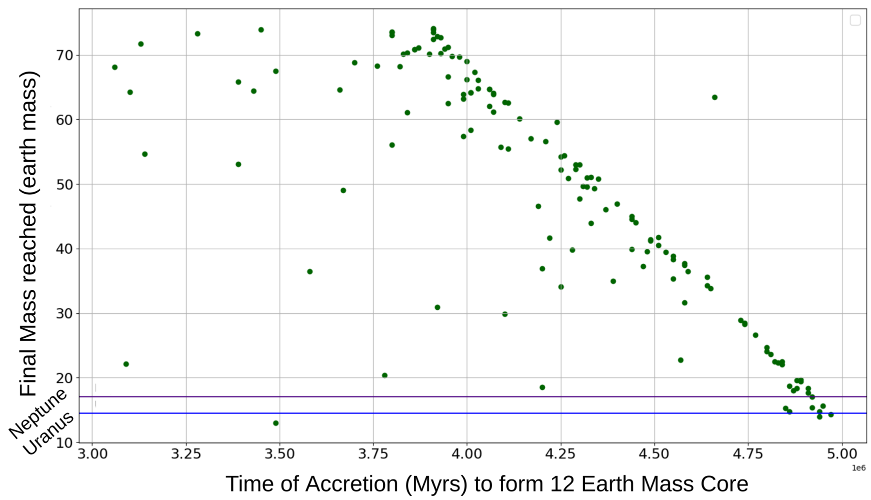

(b)

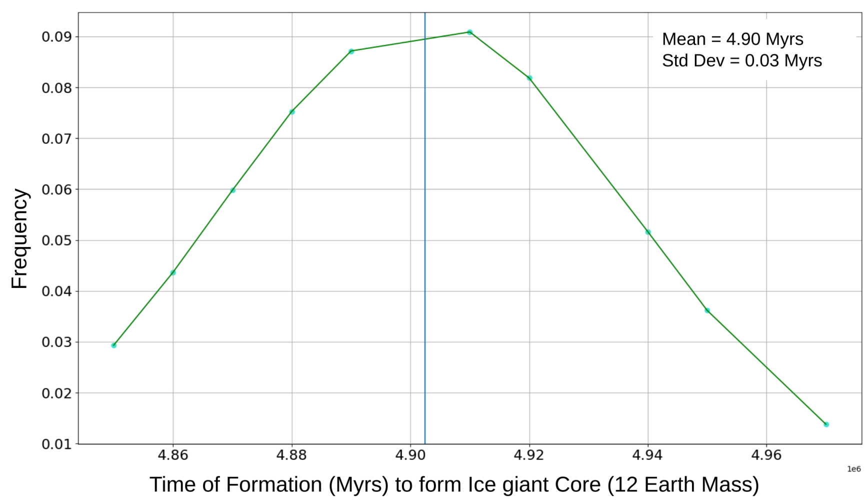

Figure 4.9: (a) Time of Accretion of $12M_{\oplus}$ core vs final mass reached. The distribution limits are between 3-5 Myrs. (b) Normal distribution fit of formation time of ice giants.

To conclude the results section, the next figure (Figure 4.10) depicts the time evolution of the orbital elements of planetesimals, cores, and planets for a selected set over a period of 5 Myrs.

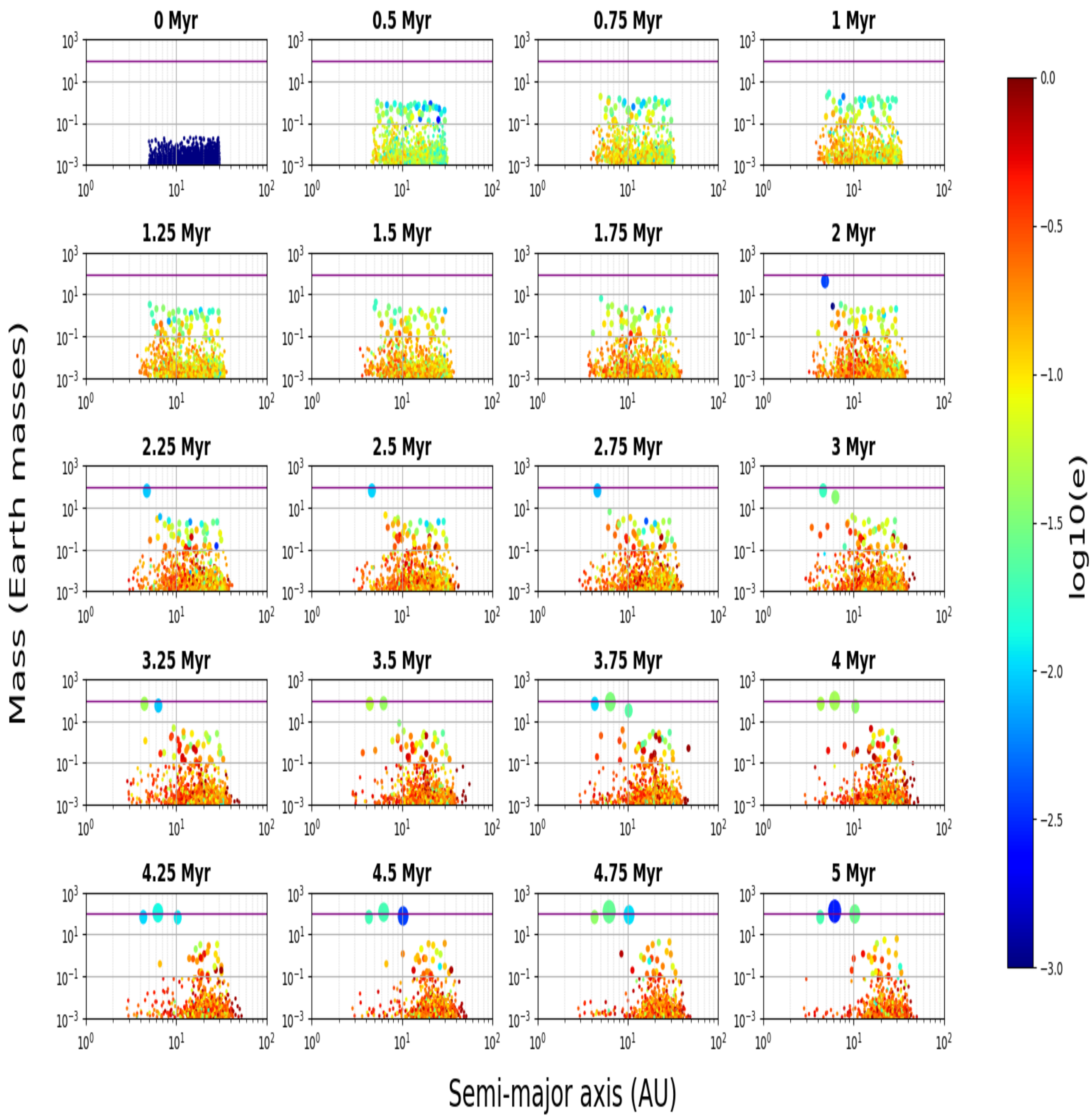

Figure 4.10: Time Evolution for one of the Production Simulation. Initial Condition: $peb\_flg = 1$, $f = 1$, $m_{\rm tot} = 4\ M_{\oplus}$, $\beta = 4.5$, $N = 1.5K$

Discussion

I verify that a particular combination of parameter values will ultimately lead to the creation of Saturn after 5 million years. The parameter values are given in the following table 5.1.

Table 5.1: Accepted Parameter values for Saturn formation

Parameter	Value
t_{diff}	$0.5\,\mathrm{Myr}$
α_{turb}	10^{-4}
b, c	$10^{8}\,\mathrm{yr}$, 3
peb_flg	1
f	0.75
m_{tot}	$4\,M_{\oplus}$
β	4.5
N	$1-5\,\mathrm{K}$
Disk Taper	Off
m_{disk}, r_{out}	$0.05M_{\odot}$, $100\,\mathrm{AU}$

It is imperative to distinguish between the outcomes of simulations conducted on systems with high and low levels of self-gravitating particles. The accompanying figure (Fig. 5.1) portrays an anomaly that arises when there are limited self-gravitating planetesimals in the system. Although the findings pertaining to the desired parameters of this investigation $(m > 10M_\oplus)$ are comparable, it is worth noting the absence of accretion for particles with masses lower than m_{tiny}, which is deemed nonphysical.

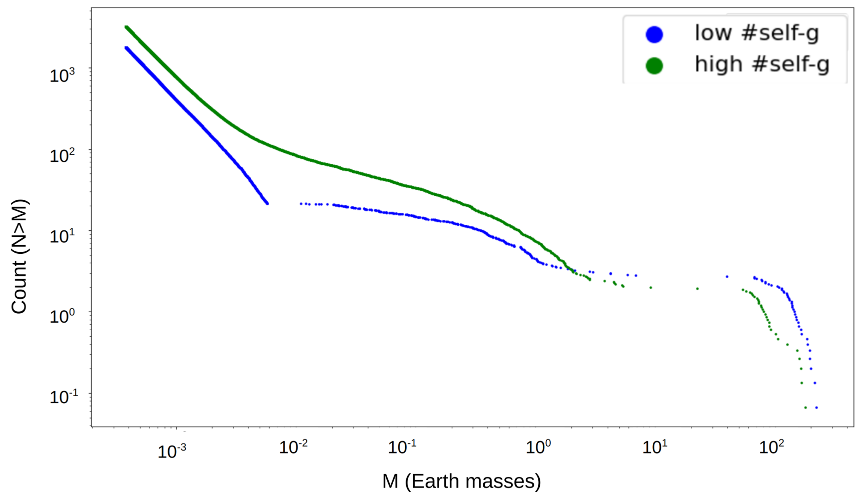

Figure 5.1: Final Size distribution for simulations with low and high number of self gravitating particles. The plot with low-self gravitating particles (green) is not physical. Initial Conditions: $m_{\text{tot}} = 4\,M_\oplus$, $f = 0.75$, $\text{peb\_flg} = 1$, $\beta = 4.5$.

In the simulations with embryo cores, I opted for Ormel's pebble accretion prescription $(\text{peb\_flg} = 1)$ due to its suitability for planetesimals and growing planets having eccentric and inclined orbits. As the growing planets migrate inwards, their eccentricities can solely be reduced through the transfer of angular momentum to smaller particles through scattering. In the absence of any particles besides the cores and pebbles in these simulations, the eccentricities persisted at high levels (see the Embryo accretion experiments), thereby enabling effective accretion with Ormel's prescription. Nonetheless, the inclusion of planetesimals in the system may render this approach ineffective, and as such, I conducted simulations employing both prescriptions in the production simulations.

5.1 Nuances in Production Simulations

The impact of five parameters, namely $\mathrm{peb\_flg}$, f, m_{tot}, N and β, on the formation of outer solar system planets was studied using production simulations. The pebble accretion formulation proposed by Ida ($\mathrm{peb\_flg} = 0$) was found to be more efficient in forming Jupiter analogues compared to Saturn analogues. However, since the study focused on the formation of Saturn, Ormel's prescription ($\mathrm{peb\_flg} = 1$) was chosen for higher probability of Saturn formation. The effect of the parameter values on ice giant formation was not significant. Similarly, the sticking efficiency was found to impact the formation probabilities of Jupiter, Saturn, and ice giants. The data presented in Figure (4.5) showed that the probability of formation of outer solar system planets was significantly impacted by varying parameter values. It should be noted that the analysis of some sets, such as those with $\mathrm{peb\_flg} = 0$ and $m_{\mathrm{tot}} = 0.5\ M_{\oplus}$, was based on a limited number of samples. Further simulations are planned to improve the statistical significance of the results presented in this study, particularly for Jupiter formation.

The initial size-frequency distributions of planetesimals have subtle differences in their effect on planet formation, despite the truncated Pareto effect. A heavier body distribution at the outset, such as with $\beta = 4.5$, increases the probability of forming gas giants compared to $\beta = 2.5$. Although statistical analysis on the effect of m_{tot} was limited, it was observed that $m_{\mathrm{tot}} = 1$ and $4\,M_{\oplus}$ were both effective for the study's purposes. The final size distributions above $10\,M_{\oplus}$ were similar for all parameters, but differences were noted below that threshold. A higher sticking efficiency ($f = 0.75/1$), pebble accretion efficiency ($\mathrm{peb\_flg} = 0$), slope ($\beta = 4.5$), and a total planetesimal mass ($m_{\mathrm{tot}} = 4\ M_{\oplus}$) produced an elevated distribution of objects between $0.1 M_{\oplus}$ and $1 M_{\oplus}$ after 5 million years. This distribution of remaining planetesimals impacts the migration of gas giants due to scattering, which in turn affects the formation of terrestrial planets.

5.2 Giant planet evolution

The selected parameter combinations produced the desired gas giants and ice giants, but their distributions in orbital elements were unique. It is noteworthy that, with $\text{peb\_flg} = 0$ and $f = 1$, where the pebble mass flux is higher, we obtain not only more giant planets, but also a wider distribution across the semi-major axis. This is due to faster accretion rates, which allows most planetesimals to grow. Conversely, with $\text{peb\_flg} = 1$ and $f = 0.75$, inward migration dominates over accretion, resulting in mostly giant planets within 10 AU and a larger population of low-mass planetesimals remaining. This suggests that these two systems will evolve differently after 5 million years.

I demonstrated that the average time for the formation of the Saturn analogues is 3.09 ± 1.33 million years. However, the precise formation time depends heavily on the specific combinations of parameters such as peb_flg, m_{tot}, and f. I lacked sufficient data points with a fixed Saturn mass range of $90 - 100\ M_{\oplus}$ to compare the effects of different parameters on its formation time. Additional simulations are necessary to make definitive conclusions. Additionally, it should be noted that these planets, particularly those formed before 3.5 million years, can be ejected from the system due to high eccentricities during their evolution.

5.3 GPU Core Accretion Simulations

The GENGA code was used to run core accretion simulations on GPU with various planetesimal populations and disk conditions for 10 million years. The Cumulative Distribution graph shown in Fig. 5.2 indicates that there were no planets larger than lunar-mass embryos, leading to the conclusion that the formation of gas giant cores was primarily due to pebble accretion rather than core accretion.

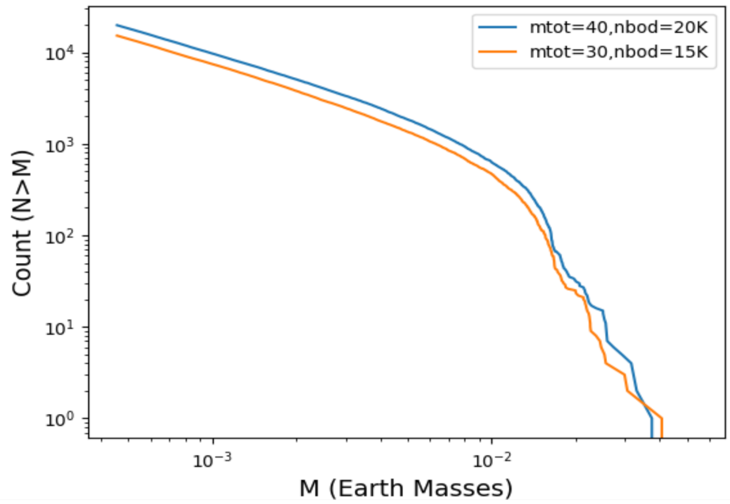

Figure 5.2: Final size distribution at 10 Myrs for Core accretion simulations: No giant planet cores were obtained

Conclusions and Future Work

The primary objective of this research was to accurately replicate the formation of Saturn within the gas disk of the outer solar system. The study yielded several fresh findings. It was posited that in the absence of a planetesimal disk, the giant planets will attain high eccentricity. It was confirmed that a particular combination of parameter values will result in the emergence of Saturn after a span of 5 million years. The process of Pebble Accretion was shown to be sensitive to various parameters and initial conditions of the disk, particularly with regards to $\mathrm{peb\_flg}$ and f, while showing limited variation in $mtot$, and β. Although N did not significantly impact the outcomes, it is worth considering the potential effects of distinguishing them based on their order of magnitude.

The results suggest that the formation of gas giants could have occurred in a sequential manner, with Jupiter, being the most massive, formed first, followed by Saturn and then the ice giants. The average formation time for Saturn is estimated to be $\langle t_{\mathrm{Saturn}} \rangle = 3.09 \pm 1.33$ Myrs, while the mean formation time for ice giants is $\langle t_{\mathrm{ice}} \rangle = 4.90 \pm 0.03$ Myrs. Notably, the formation time of Saturn aligns closely with the Hf-W reset age of the Eagle Station pallasite, which presents an opportunity for further investigation into meteorite chronology.

It proved to be a challenging task to replicate the formation of all four giant planets in the outer solar system through a single simulation. Consequently, this implies that either some crucial factor has been overlooked or further exploration of parameter space is required. Furthermore, it is possible that the remaining mass of planetesimals may impact the eccentricities of gas giants and their migration. To fully understand the influence of gas giant formation on the dynamics of the solar system, it is necessary to analyze a time span of at least 10 million years. Such an investigation should explore the presence of orbital resonances as well as the consequences of planetesimals and pebbles drifting inwardly, including their impact on the composition of the terrestrial planets.

The presented investigation relied on data derived mostly from single CPU-core runs, featuring exclusively self-gravitating particles. However, the utilization of parallel SyMBA code enables us to conduct simulations that include all planetesimals as self-gravitating entities, providing greater computational power and the ability to more accurately replicate the formation of the solar system within an expedited time-frame. Consequently, we intend to incorporate the parallel SyMBA code in forthcoming analyses for the purpose of accelerating our research outcomes.

References

1. *Our Solar System — solarsystem.nasa.gov* https://solarsystem.nasa.gov/solar-system/our-solar-system/in-depth/. [Accessed 29-Mar-2023].
2. Chambers, J. Making the Solar System. *The Astrophysical Journal* **944,** 127. https://doi.org/10.3847/1538-4357/aca96f (Feb. 2023).
3. Boss, A. P. Possible rapid gas giant planet formation in the solar nebula and other protoplanetary disks. *The Astrophysical Journal* **536,** L101 (2000).
4. Pollack, J. B. Origin and history of the outer planets: theoretical models and observational constraints. *Annual Review of Astronomy and Astrophysics* **22,** 389–424 (1984).
5. Tanaka, H. & Ida, S. Growth of a migrating protoplanet. *Icarus* **139,** 350–366 (1999).
6. Strom, S. E., Edwards, S. & Skrutskie, M. F. *Evolutionary time scales for circumstellar disks associated with intermediate-and solar-type stars* in *Protostars and planets III* (1993), 837–866.
7. Levison, H. F., Thommes, E. & Duncan, M. J. Modeling the formation of giant planet cores. I. Evaluating key processes. *The Astronomical Journal* **139,** 1297 (2010).
8. Levison, H. F., Kretke, K. A. & Duncan, M. J. Growing the gas-giant planets by the gradual accumulation of pebbles. *Nature* **524,** 322–324 (2015).
9. Matsumura, S., Brasser, R. & Ida, S. N-body simulations of planet formation via pebble accretion. *Astronomy &amp Astrophysics* **650,** A116. https://doi.org/10.1051/0004-6361/202039210 (June 2021).
10. Kruijer, T. S., Burkhardt, C., Borg, L. E. & Kleine, T. Tungsten and molybdenum isotopic evidence for an impact origin of pallasites. *Earth and Planetary Science Letters* **584,** 117440 (2022).

11. Budde, G. *et al.* Molybdenum isotopic evidence for the origin of chondrules and a distinct genetic heritage of carbonaceous and non-carbonaceous meteorites. *Earth and Planetary Science Letters* **454,** 293–303 (2016).
12. Raymond, S. N. & Izidoro, A. Origin of water in the inner Solar System: Planetesimals scattered inward during Jupiter and Saturn's rapid gas accretion. *Icarus* **297,** 134–148 (2017).
13. Fromang, S. & Lesur, G. *Angular momentum transport in accretion disks: a hydrodynamical perspective* 2017. https://arxiv.org/abs/1705.03319.
14. Matsumura, S., Brasser, R. & Ida, S. N-body simulations of planet formation via pebble accretion. *Astronomy &amp Astrophysics* **607,** A67. https://doi.org/10.1051/0004-6361/201731155 (Nov. 2017).
15. Shakura, N. I. & Sunyaev, R. A. Black holes in binary systems. Observational appearance. *Astronomy and Astrophysics* **24,** 337–355 (1973).
16. Hartmann, L., Calvet, N., Gullbring, E. & D'Alessio, P. Accretion and the evolution of T Tauri disks. *The Astrophysical Journal* **495,** 385 (1998).
17. Manara, C. F. *et al.* Evidence for a correlation between mass accretion rates onto young stars and the mass of their protoplanetary disks. *Astronomy &amp Astrophysics* **591,** L3. https://doi.org/10.1051/0004-6361/201628549 (June 2016).
18. Ida, S., Guillot, T. & Morbidelli, A. The radial dependence of pebble accretion rates: A source of diversity in planetary systems. *Astronomy &amp Astrophysics* **591,** A72. https://doi.org/10.1051/0004-6361/201628099 (June 2016).
19. Ikoma, M., Nakazawa, K. & Emori, H. Formation of Giant Planets: Dependences on Core Accretion Rate and Grain Opacity. *The Astrophysical Journal* **537,** 1013–1025. https://doi.org/10.1086/309050 (July 2000).
20. Ida, S., Tanaka, H., Johansen, A., Kanagawa, K. D. & Tanigawa, T. Slowing down type II migration of gas giants to match observational data. *The Astrophysical Journal* **864,** 77 (2018).
21. Ida, S., Muto, T., Matsumura, S. & Brasser, R. A new and simple prescription for planet orbital migration and eccentricity damping by planet–disc interactions based on dynamical friction. *Monthly Notices of the Royal Astronomical Society* **494,** 5666–5674 (2020).
22. Ormel, C. W. & Liu, B. Catching drifting pebbles-II. A stochastic equation of motion for pebbles. *Astronomy & Astrophysics* **615,** A178 (2018).

23. Ormel, C. & Klahr, H. The effect of gas drag on the growth of protoplanets-analytical expressions for the accretion of small bodies in laminar disks. *Astronomy & Astrophysics* **520,** A43 (2010).

24. Lambrechts, M. & Johansen, A. Forming the cores of giant planets from the radial pebble flux in protoplanetary discs. *Astronomy & Astrophysics* **572,** A107 (2014).

25. Safronov, V. S. *Evolution of the Protoplanetary Cloud and Formation of the Earth and the Planets* (Israel Program for Scientific Translations, 1972).

26. Kokubo, E. & Ida, S. Oligarchic growth of protoplanets. *Icarus* **131,** 171–178 (1998).

27. Aarseth, S. J. & Aarseth, S. J. *Gravitational N-body simulations: tools and algorithms* (Cambridge University Press, 2003).

28. Hernandez, D. M. & Bertschinger, E. Symplectic integration for the collisional gravitationaliNibody problem. *Monthly Notices of the Royal Astronomical Society* **452,** 1934–1944. https://doi.org/10.1093/mnras/stv1439 (July 2015).

29. Wisdom, J. & Holman, M. Symplectic maps for the n-body problem. *Astronomical Journal (ISSN 0004-6256), vol. 102, Oct. 1991, p. 1528-1538.* **102,** 1528–1538 (1991).

30. Wiegert, P., McNeil, D., Duncan, M. & Levison, H. Fast force algorithms and solar system integrations. *The Astronomical Journal* **127,** 1218 (2004).

31. Lewis, M. C., Levison, H. & Kavanagh, G. *Swiftvis: Data analysis and visualization for planetary science simulations* in *AAS/Division of Dynamical Astronomy Meeting# 38* **38** (2007), 13–11.

32. Grimm, S. L. & Stadel, J. G. The GENGA code: gravitational encounters in N-body simulations with GPU acceleration. *The Astrophysical Journal* **796,** 23 (2014).

33. Seager, S., Kuchner, M., Hier-Majumder, C. & Militzer, B. Mass-radius relationships for solid exoplanets. *The Astrophysical Journal* **669,** 1279 (2007).

34. Zaninetti, L. & Ferraro, M. On the truncated Pareto distribution with applications. *Open Physics* **6,** 1–6. https://doi.org/10.2478/s11534-008-0008-2 (Mar. 2008).